


RESEARCH

Open Access



Mechanistic study of silica nanoparticles on the size-dependent retinal toxicity in vitro and in vivo

Zhuhong Zhang^{1*} , Laien Zhao¹, Yuanyuan Ma¹, Jia Liu¹, Yanmei Huang¹, Xiaoxuan Fu¹, Shengjun Peng¹, Xiaojie Wang¹, Yun Yang¹, Xiaoyan Zhang¹, Wanru Ding¹, Jinguo Yu², Yanping Zhu¹, Hua Yan^{2*} and Shubin Yang^{3*}

Abstract

Background: Silica nanoparticles (SiO₂ NPs) are extensively applied in the biomedical field. The increasing medical application of SiO₂ NPs has raised concerns about their safety. However, studies on SiO₂ NP-induced retinal toxicity are lacking.

Methods: We investigated the retinal toxicity of SiO₂ NPs with different sizes (15 and 50 nm) in vitro and in vivo along with the underlying mechanisms. The cytotoxicity of SiO₂ NPs with different sizes was assessed in R28 human retinal precursor cells by determining the ATP content and LDH release. The cell morphologies and nanoparticle distributions in the cells were analyzed by phase-contrast microscopy and transmission electron microscopy, respectively. The mitochondrial membrane potential was examined by confocal laser scanning microscopy. The retinal toxicity induced by SiO₂ NPs in vivo was examined by immunohistochemical analysis. To further investigate the mechanism of retinal toxicity induced by SiO₂ NPs, reactive oxygen species (ROS) generation, glial cell activation and inflammation were monitored.

Results: The 15-nm SiO₂ NPs were found to have higher cytotoxicity than the larger NPs. Notably, the 15-nm SiO₂ NPs induced retinal toxicity in vivo, as demonstrated by increased cell death in the retina, TUNEL-stained retinal cells, retinal ganglion cell degeneration, glial cell activation, and inflammation. In addition, The SiO₂ NPs caused oxidative stress, as demonstrated by the increase in the ROS indicator H₂DCF-DA. Furthermore, the pretreatment of R28 cells with N-acetylcysteine, an ROS scavenger, attenuated the ROS production and cytotoxicity induced by SiO₂ NPs.

Conclusions: These results provide evidence that SiO₂ NPs induce size-dependent retinal toxicity and suggest that glial cell activation and ROS generation contribute to this toxicity.

Keywords: SiO₂ NPs, Retinal toxicity, ROS, Ganglion cell degeneration, Glial cell activation, Inflammation

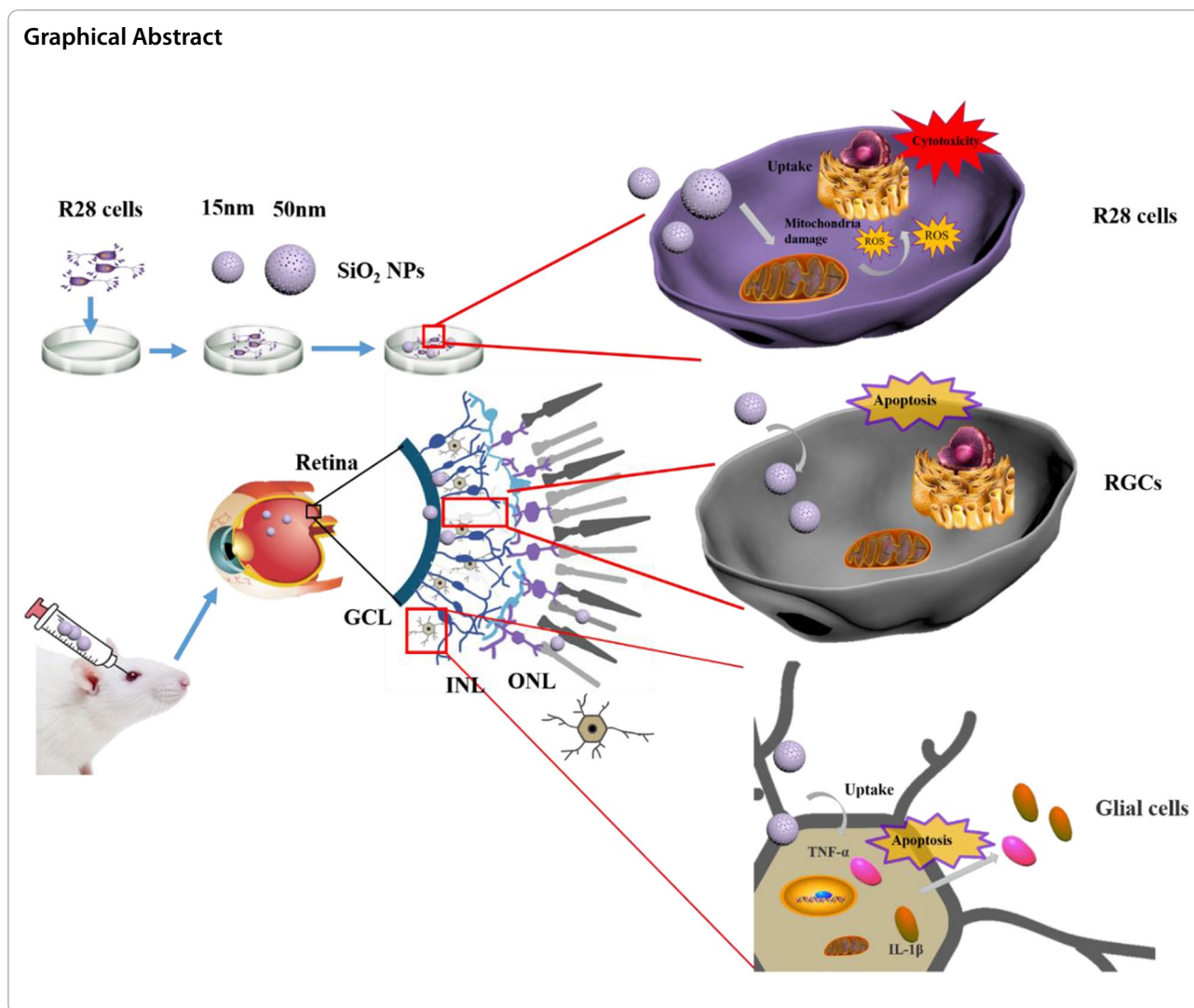
*Correspondence: zh Zhang0608@ytu.edu.cn; zyyanhuahua@tmu.edu.cn; shubinyang@ytu.edu.cn

¹ School of Pharmacy, Key Laboratory of Molecular Pharmacology and Drug Evaluation (Yantai University), Ministry of Education, Collaborative Innovation Center of Advanced Drug Delivery System and Biotech Drugs in Universities of Shandong, Yantai University, Yantai 264005, People's Republic of China

² Department of Ophthalmology, Tianjin Medical University General Hospital, Tianjin 300052, People's Republic of China

³ School of Chemistry and Chemical Engineering, Yantai University, Yantai 264005, People's Republic of China





Introduction

Due to the wide application of nanomaterials in various fields, they are being increasingly manufactured. Silica nanoparticles (SiO₂ NPs) are abundant in the Earth, and over 100 SiO₂ NP products have been released on the global market [1–3]. In the last decade, SiO₂ NPs have shown promise for applications in the biomedical field, including in disease labeling, biosensors, and the delivery of drugs and vaccines, due to their thermal stability and biocompatibility [4, 5]. Mesoporous and core/shell SiO₂ NPs have been developed for tumor imaging and therapy [6]. In addition, SiO₂ NPs have been reported for application in the treatment of ocular diseases. For example, SiO₂ NPs loaded with a nitric oxide donor can be used to treat primary open-angle glaucoma [7]. The intravitreal injection of SiO₂ NPs was shown to significantly inhibit retinal angiogenesis in oxygen-induced

retinopathy mice [8]. However, the growing potential for human exposure to SiO₂ NPs has attracted concern surrounding human health.

Some in vivo and in vitro studies have shown that SiO₂ NPs can cause toxicity to different organs in the human body; toxicity has been demonstrated in lung epithelial cells [9], liver cells [10], intestinal cells [11], the lungs [12], and kidneys [13]. In addition, SiO₂ NPs were found to induce genotoxicity and alterations in gene and protein expression [12, 14], and Chen et al. [15] reported that SiO₂ NPs can induce cornea toxicity. The local ocular delivery of medicine has become an important strategy for treating retinal diseases [16–18], and intravitreal injection has become a common treatment method for various retinal diseases including diabetic retinopathy, macular degeneration, macular edema, and inflammatory diseases [19, 20]. However, the use of intravitreal drugs

can result in retinal toxicity [21]. For example, silver nanoparticles were found to induce apoptosis in the human retinal pigment epithelia cell line ARPE-19 in vitro [22]. Wang et al. [23] reported that ZnO nanoparticles induced murine photoreceptor cell death in vitro. Nanomaterials can also induce ocular inflammation [24], and inflammation of the retinal tissue can lead to the secretion of cytokines and retinal damage. However, little is currently known about the retinal toxicity induced by SiO₂ NPs in vitro and in vivo.

The effects of nanomaterials on cells may be influenced by various properties, including the nanomaterial's crystallinity, size, shape, and surface area. Natural silica can exist in two states: crystalline and amorphous. Crystalline silica can easily lead to silicosis and lung cancer and is classified as a Group 1 carcinogen by the International Agency for Research on Cancer (IARC) [1, 25]. Notably, the toxicity of amorphous SiO₂ NPs has begun to attract the attention of scientists in recent years. Mice treated with 70-, 300-, and 1000-nm amorphous SiO₂ NPs showed no changes in hematology, histopathology, or biochemistry [26]; in contrast, Liu et al. [1] found that amorphous SiO₂ NPs induced inflammation in HUVEC cells by activating the HMGB1/TLR4/MYD88/NF- κ B signaling pathway. Tassinari et al. [27] that amorphous SiO₂ NPs induced acute toxicity in the liver and spleen of male and female rats after intravenous administration. Brandão et al. [12] demonstrated that amorphous SiO₂ NPs induced genotoxicity in lung cells. Particle size is also an important factor affecting the toxicity of SiO₂ NPs. For example, in the A549 cell line, SiO₂ NPs induced higher toxicity than SiO₂ microparticles [28]. An in vitro study showed that SiO₂ NP-induced toxicity depends not only on the particle size, but also on the cell type [29]. In the present study, we investigated the effect of amorphous SiO₂ NP size on retinal toxicity.

The mechanism of SiO₂ NP-induced toxicity remains unclear. One potential mechanism by which SiO₂ NPs might induce retinal toxicity involves reactive oxygen species (ROS). Some reports have suggested that SiO₂ NPs can induce ROS production in various cell lines, including human keratinocytes [30], human HK-2 cells [31], and HUVEC cells [1]. Many studies have indicated that ROS are closely related to cytotoxicity [32, 33], and the inhibition of ROS can ameliorate the cytotoxicity. Other studies have demonstrated that SiO₂ NPs can induce inflammation [11], and oxidative stress and inflammation are thought to be closely related to the toxicity induced by nanoparticles.

Previous studies generally focused on a limited number of endpoints; in contrast, in the current study, we implemented a comprehensive set of tests to assess the potential effects of SiO₂ NPs on the retina and retinal

cells. More specifically, the cytotoxicity, morphological changes, and localization of SiO₂ NPs in R28 cells induced by SiO₂ NPs with two different sizes (15 and 50 nm) were investigated. We also determined the role of SiO₂ NPs in the apoptosis of retinal cells and the damage of retinal ganglion cells (RGCs). In addition, we explored the potential role of glial cell activation, inflammation and ROS accumulation in SiO₂ NP-induced retinal toxicity.

Materials and methods

Chemicals and reagents

SiO₂ NPs were purchased from Shanghai Macklin Biochemical Co., Ltd (Shanghai, China). Fetal bovine serum (FBS), Dulbecco's modified eagle medium (DMEM), and penicillin/streptomycin were obtained from Life Technologies (Carlsbad, CA, USA). N-acetylcysteine (NAC) and 2',7'-dichlorofluorescein diacetate (H₂DCF-DA) were purchased from Sigma-Aldrich (St. Louis, MO, USA). A JC-1 mitochondrial membrane potential assay kit was purchased from Beyotime Biotechnology Co., Ltd. (Shanghai, China).

Characterization of SiO₂ NPs

The sizes and morphologies of the SiO₂ NPs were evaluated by transmission electron microscopy (TEM; Tecnai F20, Philips, Netherlands, 200 kV) and field-emission scanning electron microscopy (FE-SEM; JEOL JSM-7001F). The crystal structures of the SiO₂ NPs were examined by powder X-ray diffraction (XRD) using monochromic Cu-K α radiation (Rigaku Smart Lab, Japanese Neo Confucianism, Japan) at 40 kV and 300 mA. To investigate the chemical states of the SiO₂ NPs an X-ray photoelectron spectrophotometer (XPS) was employed. XPS analyses of the nanoparticles were conducted by Axis Ultra DLD instrument (Kratos Analytical, Manchester, UK).

Size and stability characterization of SiO₂ NPs in cell culture medium

Due to concerns about the interaction between medium components, serum and SiO₂, the stability of SiO₂ NPs in cell culture media was investigated. SiO₂ NPs were suspended at a concentration of 100 μ g/ml in DMEM media with 10%, 1% or without FBS, and ultrapure water for 12 and 24 h in a humidified incubator prior to Hydrodynamic diameter and Zeta (ζ) potential analysis, which were measured using Zetasizer Nano (Malvern, Worcestershire, UK).

Cell culture and treatment with SiO₂ NPs

The retinal precursor cell line R28 was obtained from Kerfast (Boston, MA, USA) and cultured according

to the supplier's instructions. The cells were cultured in DMEM+, which contained 420 mL DMEM (Sigma-Aldrich, St. Louis, MO, USA), 15 mL sodium bicarbonate (Sigma-Aldrich, St. Louis, MO, USA), 50 mL calf serum (Hylone), 5 mL MEM non-essential amino acids (GIBCO), 5 mL L-glutamine (GIBCO), and 0.625 mL Gentamicin (80 mg/mL; Solarbio Life Sciences Co., Ltd, Beijing, China). The cells were maintained at 37 °C in a humidified atmosphere containing 5% CO₂. The human retinal pigment epithelial cell line (ARPE-19 cells) was purchased from the Fu Heng Cell Center (Shanghai, China). The cells were cultured in DMEM/F-12 medium (GIBCO) containing 10% FBS, penicillin (50 U/mL), and streptomycin (50 U/mL). Cells were cultured at 37 °C in a humidified atmosphere with 5% CO₂. SiO₂ NPs were dispersed in ultrapure water to prepare a stock solution (200 mg/mL). The stock solution was sonicated using a probe sonicator (Ningbo Xinzhi Biotechnology Co., Ltd., Ningbo, China) at 600 W for 40 min (pulse on: 2 s and pulse off: 2 s in an ice-bath) and diluted to different concentrations with culture medium just before cell exposure. The cells were adjusted to a concentration of 1×10^5 cells/mL in a volume of 100 µL per well in 96-well plates for toxicity assays. NP suspensions were freshly prepared before the treatments, and diluted to various concentrations with the FBS-free culture medium, then immediately applied to the cells.

Measurement of cellular ATP levels and lactate dehydrogenase (LDH) release

Cell Titer-Glo[®] Luminescent Cell Viability Assay (Promega, Madison, WI, USA) was used to monitor the ATP levels in SiO₂ NP-treated ARPE-19 or R28 cells according to the manufacturer's instructions. Briefly, cells were cultured in 96-well plates and hatched overnight. After the cells were adhered, 15 and 50-nm SiO₂ NPs were added in a dose-dependent manner (0, 5, 10, 20, 40, and 80 µg/mL) into the culture medium and cultured for 12 or 24 h. After washed off the culture medium with PBS, 100 µL of Cell Titer-Glo reagent was added per well. Cells were incubated at 37 °C in 5% CO₂ for 10 min, and luminescence was recorded using a Synergy H4 Hybrid microplate reader (BioTek, Winooski, USA). Cellular ATP levels were calculated by comparing the luminescence intensity of the treated cells to that of the vehicle control. The cytotoxicity of SiO₂ NPs was assessed using the LDH Release Assay (Beyotime, Beijing, China) as our previous method [34]. The absorbance was detected at a wavelength of 490 nm by using a Synergy H4 Hybrid microplate reader and data are presented as relative values compared to control.

Cell morphology

R28 cells were seeded in 96-well plates at a density of 1×10^4 cells/well and cultured overnight in a CO₂ incubator. The cells were exposed to SiO₂ NPs at different concentrations (5–80 µg/mL) for 12 and 24 h. The changes in cell morphology were examined using a phase-contrast microscope (Leica DM16000B, Heidelberg, Germany).

Uptake of SiO₂ NPs

To examine the localization of SiO₂ NPs in R28 cells, R28 cells were plated in six-well plates, cultured overnight, and treated with SiO₂ NPs (20 µg/mL) for 24-h. The R28 cells were then collected, washed three times with phosphate-buffered saline (PBS), and fixed with 2.5% glutaraldehyde solution at 4 °C overnight. After the fixed cells were dehydrated, serial ultrathin sections were created and examined by TEM (Hitachi H7650, Japan).

Detection of mitochondrial membrane potential

The SiO₂ NP-induced changes in mitochondrial membrane potential were assessed as previously described [34]. Briefly, R28 cells were seeded in dishes at a density of 1×10^5 cells/mL and cultured overnight. The cells were treated with different concentrations of SiO₂ NPs for 6, 12 and 24 h. Following treatment, the cells were washed three times with PBS and then incubated with JC-1 (20 µM; Beyotime, Beijing, China) for 15 min. After removing the JC-1 staining solution, the cells were washed three times, and PBS was added for imaging by confocal laser scanning microscopy (CLSM; ZEISS LSM 800, Germany).

Intravitreal injection of SiO₂

Three-week-old male Sprague–Dawley rats were purchased from Pengyue Experimental Animal Company (Jinan, China). All animal procedures were carried out in accordance with the National Institutes of Health Guide for the Care and Use of Laboratory Animals and were in compliance with the ARVO Statement for the Use of Animals in Ophthalmic and Vision Research. Animal protocols were approved by the Committee of Yantai University for the Care and Use of Laboratory Animals. All rats were housed under 12-h dark/light cycles at 23 °C ± 1 °C, and food and water were available ad libitum. Prior to intravitreal injection, the rats were anesthetized via the intraperitoneal injection of ketamine (100 mg/kg) and xylazine (7 mg/kg), and the pupils were anesthetized with 0.5% proxymetacaine hydrochloride. The rats were randomly divided into three groups: sham, vehicle control (PBS), and SiO₂ NPs. Intravitreal injections were carried out using a 30-gauge needle attached to a 1-mL syringe; 5 µL of SiO₂ NP suspension was injected to obtain a final concentration of 80 µg/mL in the vitreous humor.

TUNEL assay

Assays were performed using a one-step TUNEL Apoptosis Assay Kit (Beyotime) following the manufacturer's instructions. Briefly, cryosections were stained using the kit to test DNA fragmentation as an indicator of cell death. To count TUNEL-positive cells, three sections from each rat were imaged by confocal laser scanning microscopy (CLSM; ZEISS LSM 800, Germany). The counts from all sections of the same animal were averaged, and the data from six rats were used to obtain the average and standard deviation (SD) for the group.

Evaluation of retinal ganglion cells (RGCs) and inflammatory markers in SiO₂ NP-injected retinas by immunofluorescence

Immunostaining was performed following the previously described method. Briefly, cryosections were permeabilized with 0.5% Triton X-100 in PBS for 15 min, blocked with 5% bovine serum albumin (BSA) for 1 h at room temperature, and then stained with primary antibodies in blocking solution overnight at 4 °C prior to incubation with secondary antibodies diluted in blocking solution for 1 h at room temperature. Nuclei were stained with 4',6-diamidino-2-phenylindole (DAPI). The primary antibodies were as follows: mouse anti- β -III-tubulin (1:100, Beyotime), rabbit anti-gial fibrillary acid protein (anti-GFAP; 1:100, Beyotime), rabbit anti-TNF- α (1:100, Beyotime), and IL-1 β (1:100, Beyotime). To quantify immunofluorescence intensity, the areas of β -III-tubulin and GFAP immunopositivity were determined by thresholding based on the images obtained using Image J (National Institutes of Health, Bethesda, MD, USA). TNF- α - and IL-1 β -positive cells were quantified from at least three sections of each rat. Each group included six rats. Comparisons between groups were made using one-way analysis of variance (ANOVA).

Measurement of ROS

Intracellular ROS production was assessed using H₂DCF-DA staining as previously described [34]. Briefly, R28 cells were treated with 10 μ M H₂DCF-DA for 30 min in the cell culture incubator. The cells were washed with PBS to remove unincorporated dye and then treated with 5–80 μ g/mL SiO₂ NPs in phenol red-free medium. The cells were incubated for 24 h, and the fluorescence intensity was measured after 2, 4, 6, 12, and 24 h using a Synergy H4 Hybrid microplate reader. Meanwhile, the oxidation of H₂DCF-DA was detected by CLSM (ZEISS LSM 800, Germany) at the same time points.

Statistical analysis

All data are presented as the mean \pm SD. Statistical analysis was performed using Graph Pad Prism 6 (La Jolla,

CA, USA). Treatment-related differences were evaluated by one-way ANOVA followed by Dunnett's tests (for comparisons of different concentrations to the vehicle control) or by two-way ANOVA followed by Tukey's multiple comparison test (for comparisons of two treatment groups in NAC pretreatment experiments). A difference was considered statistically significant when the *p* value was less than 0.05.

Results

Characterization of SiO₂ NPs

The wide application of SiO₂ NPs in the biomedical field has raised concerns regarding the safety of these NPs in humans and the environment. While the cytotoxicity of SiO₂ NPs has been investigated by numerous scientists [3, 5, 35], most of these studies explored various SiO₂ NP characteristics using a wide variety of in vitro models. Until now, limited studies have evaluated the retinal toxicity both in vitro and in vivo. In the present study, we explored the retinal toxicity of two types of SiO₂ NPs with different sizes both in vitro and in vivo. We also investigated the potential mechanism underlying the retinal toxicity induced by SiO₂ NPs.

Recently, SiO₂ NPs have shown great potential in the treatment of ocular diseases [36–39]. Given the widespread use of SiO₂ NPs to treat ocular diseases, the ocular toxicity of SiO₂ NPs requires more attention from scientists and ophthalmologists. Park et al. reported that SiO₂ NPs with sizes of 50, 100, and 150 nm did not induce significant cytotoxicity in cultured human corneal epithelial cells [40]. However, Chen et al. reported that SiO₂ NPs led to cytotoxicity, ROS generation, and DNA damage in the human cornea [15]. SiO₂ NPs can be used as intravitreal drug carriers [38, 41]; however, to the best of our knowledge, the retinal toxicity of SiO₂ NPs has not been investigated before now. Therefore, we conducted both in vitro and in vivo experiments to evaluate the retinal toxicity of SiO₂ NPs with sizes of 15 and 50 nm. The in vitro study used human R28 retinal precursor cells, which are expected to mimic in vivo responses.

We first evaluated the effect of SiO₂ NP size on retinal toxicity. The morphology, size, and structure of SiO₂ NPs were characterized by SEM, TEM, and XRD, respectively. The SEM images of the two types of SiO₂ NPs (Fig. 1A and B) indicate that both NPs had spherical morphologies. The TEM images (insets of Fig. 1A and B) show that the SiO₂ NPs had sizes of approximately 15 and 50 nm and were slightly aggregated in aqueous solution. As shown in Fig. 1C and D, the XRD patterns confirmed the amorphous nature of the 15 and 50 nm SiO₂ NPs. There is no Bragg peak observed. The diffraction pattern of SiO₂ NPs exhibited a single broad peak centered

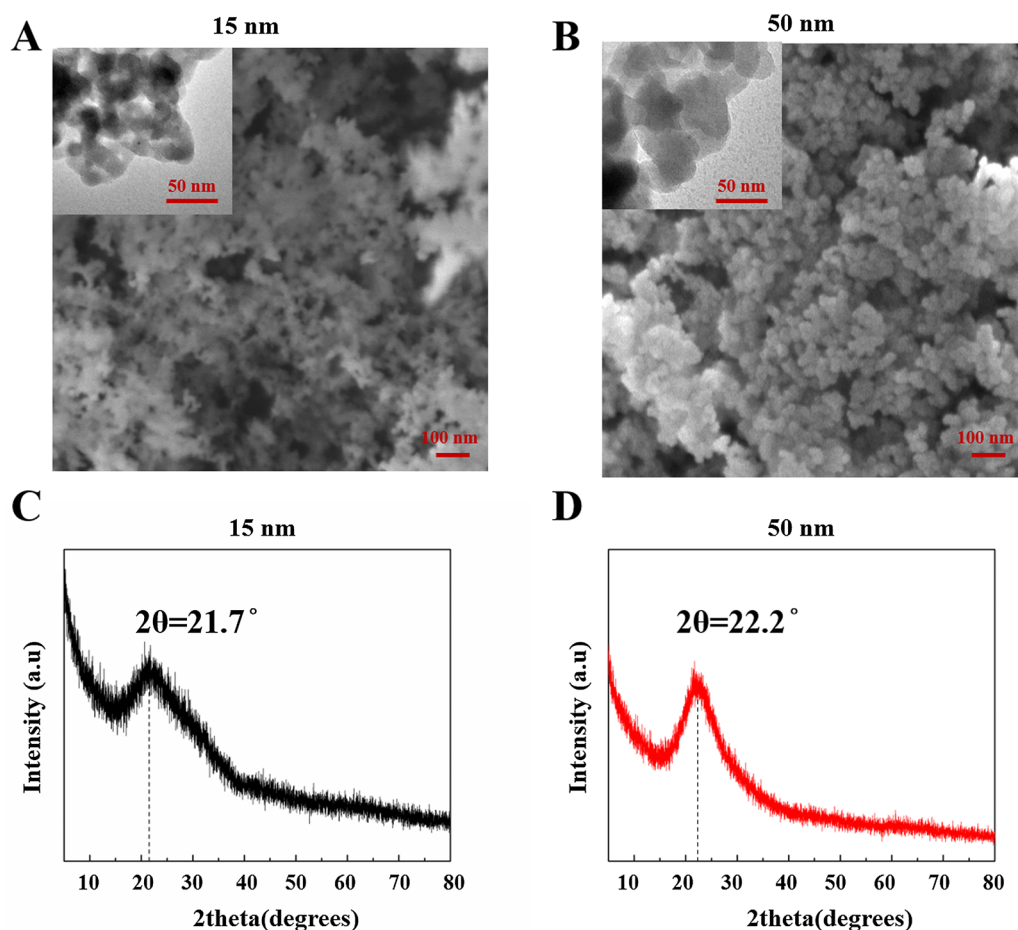


Fig. 1 Characterization of SiO₂ NPs. SEM and TEM (insets) images of **(A)** 15-nm SiO₂ NPs and **(B)** 50-nm SiO₂ NPs. XRD spectra of 15-nm SiO₂ NPs **(C)** and 50-nm SiO₂ NPs **(D)**

at $\sim 22^\circ$, which is the characteristic peak for amorphous SiO₂ NPs.

In order to investigate the chemical state of the elements of SiO₂ NPs, XPS was performed. The wide-scan XPS survey spectrum of the NPs validates the existence of Si and O atoms, consistent with other studies. The high-resolution XPS spectrum of Si2p for both samples displayed two peaks, which indicated the main peak presented as Si (IV), and the other peak was matched well with Si (III), which was only a small amount. These results were consistent with other studies (see, for example, ref [42]). The O (1 s) spectra for both samples showed two peaks (Fig. 2). The main peak around 533eV was matched to the O²⁻ of SiO₂, and the other peak at 534.9 eV can be fitted to the weakly bonded oxygen of water molecules adsorbed on the surface of NPs and possibly the OH functional group of SiO₂, which is similar to other reports [43, 44]

To investigate about the aggregation of the SiO₂ NPs by FBS and cell culture medium, the Hydrodynamic

size and Zeta-Potential of SiO₂ NPs in different suspensions (ultrapure water, DMEM, DMED+1%FBS and DMEM+10%FBS) were measured at 12 h and 24 h of incubation. As shown in Table 1, both 15- and 50-nm SiO₂ NPs aggregated to various degrees in different suspensions. NPs slightly aggregated in water and DMEM suspensions. It is obvious that FBS can promote the aggregation of NPs more than DMEM. And, this effect was dose-dependent. Especially when the FBS content was increased to 10%, the phenomenon became more prominent, and the hydrodynamic size of both NPs in the medium+10% FBS suspension was 2–3 times larger than that in water. In contrast, the hydrodynamic size of the FBS-free DMEM suspension is very similar to that of the water suspension. Consistent with this, changes in ζ potential also confirmed the aggregation phenomena (Table 2). Assessing the surface charge and stability of NPs are two widely uses of ζ potential [45]. Table 2 showed the ζ potential measurements of 15- and 50-nm SiO₂ NPs in different kinds of suspension. The ζ potential

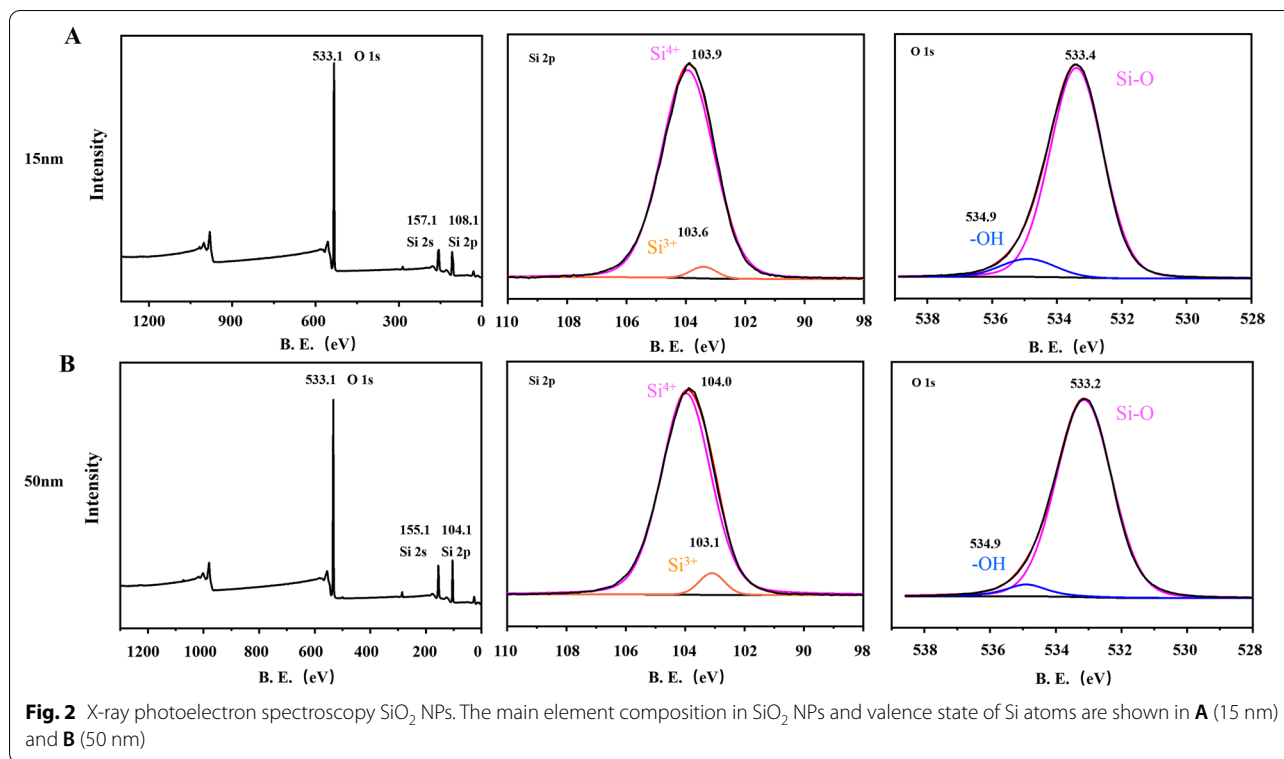


Table 1 The Hydrodynamic Diameter of SiO_2 NPs in different suspensions

Size (nm)	Time (hour)	Ultrapure water	DMEM	DMEM + 1% FBS	DMEM + 10% FBS (nm) ^a
15	12	140.3 ± 7.5	140.6 ± 4.8	178.9 ± 10.9	364.6 ± 14.1
	24	153.7 ± 31.3	150.6 ± 6.7	165.6 ± 3.6	381.7 ± 7.6
50	12	239.0 ± 1.7	254.8 ± 4.0	260.4 ± 4.0	381.3 ± 24.7
	24	252.8 ± 22.8	260.7 ± 8.9	243.0 ± 6.4	434.4 ± 12.5

^a Data are expressed as mean ± standard deviation (SD)

values of all samples ranged from -6 mV to -20 mV. This is similar with one study [46], which the potential values were negative. Our own results showed that the potential values of ultrapure water and FBS-free DMEM ranged from -10 mV to -20 mV, which can be considered as a relatively stable state [45]. However, ζ potential values of DMEM + 10% suspension changed to a highly unstable state ($0 \sim -10$ mV) [47]. Notably, in our study, this aggregation was not time-dependent. Hence, to avoid the effect of this aggregation induced by FBS on toxicity, in the following in vitro assays, we used the FBS-free medium to disperse the NPs and sonicated for 40 min in ice-bath before all the treatments.

Cytotoxicity of SiO_2 NPs in R28 and ARPE-19 cells

We compared the cytotoxicity of the SiO_2 NPs with different sizes (15 and 50 nm) in two cell lines, which are human R28 retinal precursor cells and ARPE-19 human retinal pigment epithelial cells. Cytotoxicity was determined by adenosine triphosphate (ATP) assay and lactate dehydrogenase (LDH) release assay. The R28 and ARPE-19 cells were treated with the two types of SiO_2 NPs at various concentrations ranging from $5\text{--}80$ $\mu\text{g}/\text{mL}$ for 12 and 24 h. SiO_2 NPs are much more toxic to R28 than to ARPE-19. As shown in Fig. 3, the SiO_2 NPs induced significant time- and concentration-dependent decreases in ATP content (Fig. 3A & B) and LDH release (Fig. 3C & D). Among the two types of SiO_2 NPs, the R28 cells showed higher sensitivity to the 15-nm SiO_2 NPs. Furthermore, SiO_2 NPs are much

more toxic to R28 cells than to ARPE-19 cells (Additional file 1: Figure S1). Quantitative analysis showed that exposure of R28 cells to 15-nm NPs at a concentration of 20 $\mu\text{g}/\text{mL}$ for 12 h resulted in a significant decrease in ATP content. However, ARPE-19 cells were exposed to 15 nm nanoparticles at a concentration of 80 $\mu\text{g}/\text{mL}$ for 12 h to induce a similar phenomenon. The results from LDH release assay further confirmed this. Thus, in the following studies, our *in vitro* assays were all performed in R28 cells.

SiO₂ NPs induce morphological changes in R28 cells

The morphology of the R28 cells changed as the SiO₂ NP concentration increased. After 12 h, the cell morphology became irregular when the NP concentration reached 20 (50-nm SiO₂ NPs; Fig. 4A) or 40 $\mu\text{g}/\text{mL}$ (50-nm SiO₂ NPs; Fig. 4A). At 24 h, the changes in cell morphology became more prominent with increasing SiO₂ NP concentration (Fig. 4B). At the concentration of 80 $\mu\text{g}/\text{mL}$, most cells were detached, and the density was obviously reduced.

In vitro localization of SiO₂ NPs in R28 cells

The *in vitro* distributions of SiO₂ NPs with sizes of 15 and 50 nm in R28 cells were evaluated by TEM. In R28 cells before SiO₂ NP treatment, no SiO₂ NPs were observed in the nucleus or cytosol (red arrows) (Fig. 5). After exposure for 24 h, both 15- and 50-nm SiO₂ NPs were visible in the cytoplasm, and some 15-nm SiO₂ NPs were found in the mitochondria. Furthermore, nuclei were shrunken in cells treated with NPs.

SiO₂ NPs induce mitochondrial dysfunction

As the 15-nm SiO₂ NPs accumulated in the mitochondria, we measured the change in mitochondrial depolarization ($\Delta\Psi\text{m}$) in R28 cells treated with 15-nm SiO₂ NPs. The value of $\Delta\Psi\text{m}$ was measured using JC-1 dye. The R28 cells were treated with SiO₂ NPs at concentrations of 20, 40, and 80 $\mu\text{g}/\text{mL}$ for 6, 12, and 24 h. Decreases in mitochondrial depolarization in the R28 cells were observed as early as 6 h after treatment with 80 $\mu\text{g}/\text{mL}$ SiO₂ NPs (Fig. 6A). As shown by the JC-1 staining images (Fig. 6C),

the transition from red fluorescence to green fluorescence became more obvious at 24 h after treatment, suggesting that the SiO₂ NPs induced a significant time- and concentration-dependent decrease in mitochondrial depolarization (Fig. 6). Consequently, in subsequent experiments, the SiO₂ NP concentration of 80 $\mu\text{g}/\text{mL}$ was used to investigate the retinal toxicity *in vivo*.

SiO₂ NPs induce retinal toxicity in vivo

To examine the retinal toxicity of SiO₂ NPs *in vivo*, SiO₂ NPs were intravitreally injected. At 1, 7, and 14 d after injection, the rats were euthanized, and frozen sections of the retina were prepared for fluorescence staining. The retina shape became irregular at 7 d after injection, and the retinas became very loose at 14 d after injection. Notably, many cells infiltrated into the retinal ganglion cell layer (GCL); these cells were suspected to be inflammatory cells. To measure retinal cell death after SiO₂ NP injection, cells stained with DAPI were counted in the outer nuclear layer (ONL), inner nuclear layer (INL), and GCL. The number of cells decreased with time after injection in the ONL, INL, and GCL, and the overall number of cells also decreased (Fig. 7). Next, retinal cryosections were analyzed by TUNEL apoptosis assay (Fig. 8). The percentage of apoptotic cells increased in the SiO₂ NP-treated groups in a time-dependent manner. Compared to the sham group, the intravitreal injection of SiO₂ NPs increased the number of TUNEL-positive cells by approximately 4-, 16-, and 32-fold after 1, 7, and 14 d, respectively.

SiO₂ NPs activate the inflammatory response in vivo

As mentioned above, cells that we suspected to be inflammatory cells infiltrated the GCL. Thus, we investigated whether the SiO₂ NPs caused retinal inflammation. GFAP, a marker of glial cells in the retina, was assessed by immunofluorescence staining. As demonstrated in Fig. 9, glial cells were obviously activated as early as 1 d after the injection of SiO₂ NPs, and the number of activated glial cells rose sharply at 7 d after injection (Fig. 9A and B). The maximum GFAP signal induction was approximately 60 times that of the PBS control at 14 d after injection

Table 2 The Hydrodynamic Diameter of SiO₂ NPs in different suspensions

Size (nm)	Time (hour)	Utrapure water	DMEM	DMEM + 1% FBS	DMEM + 10% FBS (nm) ^a
15	12	-19.4 ± 1.2	-12.6 ± 1.2	-16.4 ± 0.8	-6.8 ± 0.3
	24	-17.4 ± 0.1	-13.6 ± 1.7	-17.6 ± 1.5	-6.7 ± 1.0
50	12	-15.7 ± 0.2	-11.8 ± 1.7	-10.0 ± 0.5	-6.6 ± 1.1
	24	-13.3 ± 0.7	-13.0 ± 1.1	-9.2 ± 2.6	-6.7 ± 0.8

^a Data are expressed as mean ± standard deviation (SD)

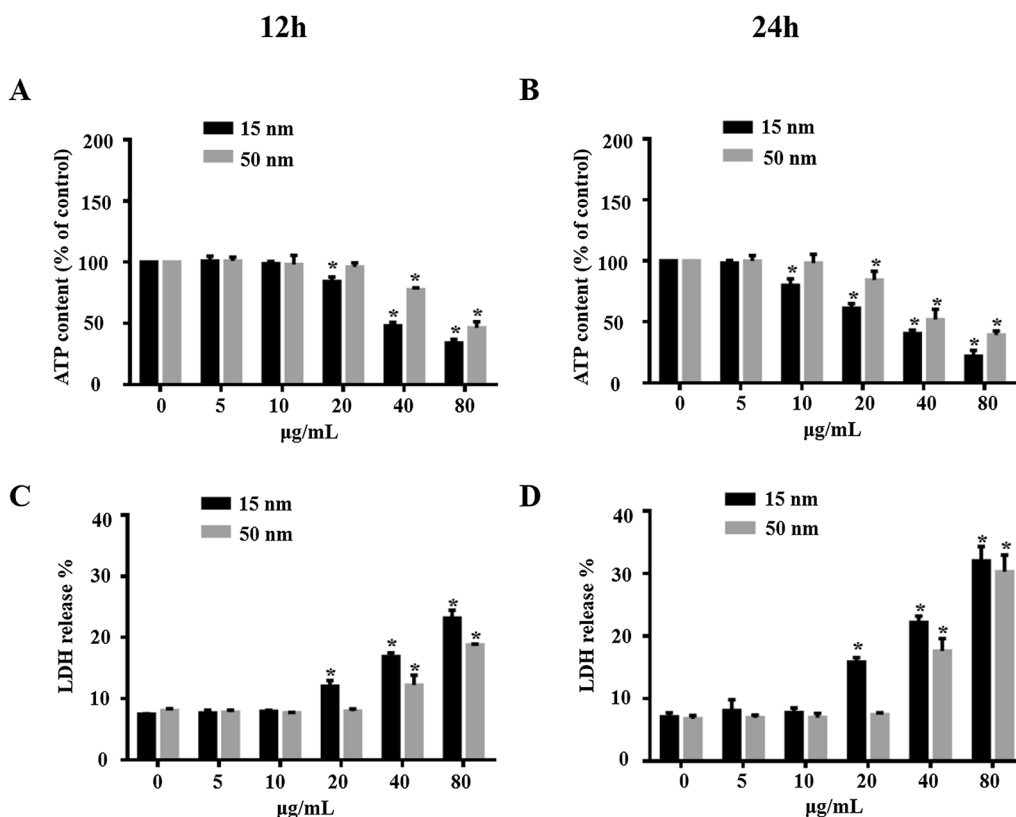


Fig. 3 SiO₂ NPs induce cytotoxicity in R28 cells. R28 cells were exposed to different concentrations (5–80 µg/mL) of SiO₂ NPs for (A and C) 12 h and (B and D) 24 h before measurements of (A and B) ATP content and (C and D) LDH release. Data points represent the mean ± SD from three independent experiments with three samples per concentration in each experiment. **p* < 0.05 compared to the control

(Fig. 9C). RGCs can be damaged by various stimuli such as inflammation, ischemia, oxidative stress, and excitotoxicity [48]. Therefore, to understand whether the activation of glial cells can damage RGCs, we evaluated the expression of β -III-tubulin, a marker of RGCs. As shown in Fig. 9A, at 1 d after SiO₂ NP injection, the RGCs (β -III-tubulin positive) were reduced by 52% compared to the vehicle control. The cell number decreased more predominantly at 7 and 14 d after injection (Fig. 9B & C). These findings demonstrate that the intravitreal injection of SiO₂ NPs activated glial cells and damaged RGCs.

As SiO₂ NPs have been demonstrated to induce inflammation in HUVEC cells [1], and pro-inflammatory cytokines (e.g., TNF- α and IL-1 β) secreted by macrophages play a crucial role in the inflammation process, we investigated whether the SiO₂ NPs induced the secretion of TNF- α and IL-1 β . The retinas were stained with antibodies against TNF- α and IL-1 β and assessed by immunofluorescence staining. The levels of TNF- α and IL-1 β were notably increased in the group injected with SiO₂ NPs compared to the control. For example, the number of IL-1 β -positive cells increased by 8- and

23-fold compared to the vehicle control at 1 and 7 d after SiO₂ NP injection, respectively (Fig. 10A and C); the number of TNF- α -positive cells showed similar trends (Fig. 10B and D).

Taken together, the above results indicate that the SiO₂ NPs caused retinal cell death and activated retinal inflammation.

SiO₂ NPs cause ROS overproduction

Driven by the in vitro and in vivo effects of SiO₂ NPs on cell viability, morphology, mitochondrial dysfunction, apoptosis, and inflammation, we investigated the potential mechanisms underlying the retinal toxicity of SiO₂ NPs. Previous studies demonstrated that one of the main toxicity mechanisms of NPs involves ROS generation [15, 23, 49]. Therefore, we first investigated whether the 15- and 50-nm SiO₂ NPs induced oxidative stress. R28 cells were treated with SiO₂ NPs at concentrations ranging from 5 to 80 µg/mL, and ROS production was monitored at 2, 4, 6, 12, and 24 h after treatment (Fig. 11). The SiO₂ NPs were found to have size-, time-, and concentration-dependent effects on ROS generation. Compared

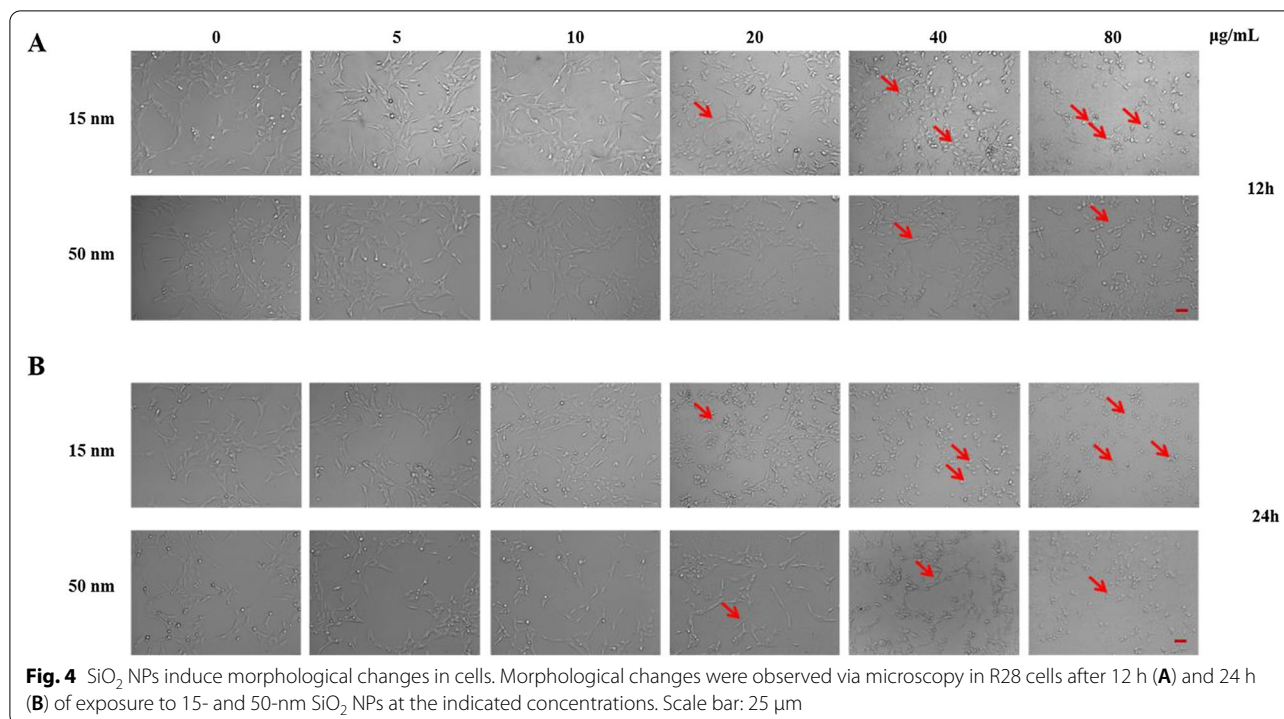


Fig. 4 SiO₂ NPs induce morphological changes in cells. Morphological changes were observed via microscopy in R28 cells after 12 h (A) and 24 h (B) of exposure to 15- and 50-nm SiO₂ NPs at the indicated concentrations. Scale bar: 25 µm

with the control group, the ROS levels increased significantly within 2 h of treatment with 15-nm SiO₂ NPs at 80 µg/ml. The ROS level continued to increase dramatically over time, reaching a maximum value (approximately 3 times that of the control group) at 4 h after treatment with 15-nm SiO₂ NPs (Fig. 11A). Similarly, the ROS level increased significantly at 6 h after treatment with 50-nm SiO₂ NPs (80 µg/mL); the maximum ROS level (2.3 times that of the control) occurred at 6 h after treatment (Fig. 11C). The ROS levels then decreased from 6 h to 12 and 24 h after treatment, presumably due to reduced cell growth (Fig. 3). To further verify the ROS generation results, we performed ROS fluorescence staining. R28 cells were treated with 15- and 50-nm SiO₂ NPs at concentrations of 20 and 80 µg/mL. The CLSM images show that the ROS levels increased with incubation time (Fig. 11B and D). The increase in ROS level suggests that treatment with SiO₂ NPs resulted in oxidative stress. Subsequent assays focused on the 15-nm SiO₂ NPs.

SiO₂ NP-induced retinal toxicity is attenuated by ROS scavenging

To further investigate the role of ROS generation in the retinal toxicity of SiO₂ NPs, we used NAC, a ROS scavenger, to inhibit intracellular ROS generation. R28 cells were pretreated with NAC (10 mmol) for 1 h prior

to treatment with SiO₂ NPs (5–80 µg/ml) for 12 h. As shown in Fig. 12A, NAC significantly attenuated ROS induction. To further verify this result, we performed ROS fluorescence staining. The CLSM images show that pretreating cells with NAC before treatment with 40 µg/mL SiO₂ NPs inhibited ROS production (Fig. 12B). Finally, the pretreatment of cells with NAC significantly decreased SiO₂ NP-induced retinal toxicity in the R28 cells, as evidenced by the reduction in ATP content (Fig. 12C). These findings indicate that SiO₂ NP-induced retinal toxicity was partially mediated by ROS generation.

Discussion

The wide application of SiO₂ NPs in the biomedical field has raised concerns regarding the safety of these NPs in humans and the environment. While the cytotoxicity of SiO₂ NPs has been investigated by numerous scientists [3, 5, 35], most of these studies explored various SiO₂ NP characteristics using a wide variety of in vitro models. Until now, no study has evaluated the retinal toxicity either in vitro or in vivo. In the present study, we explored the retinal toxicity of two types of SiO₂ NPs with different sizes both in vitro and in vivo. We also investigated the potential mechanism underlying the retinal toxicity induced by SiO₂ NPs.

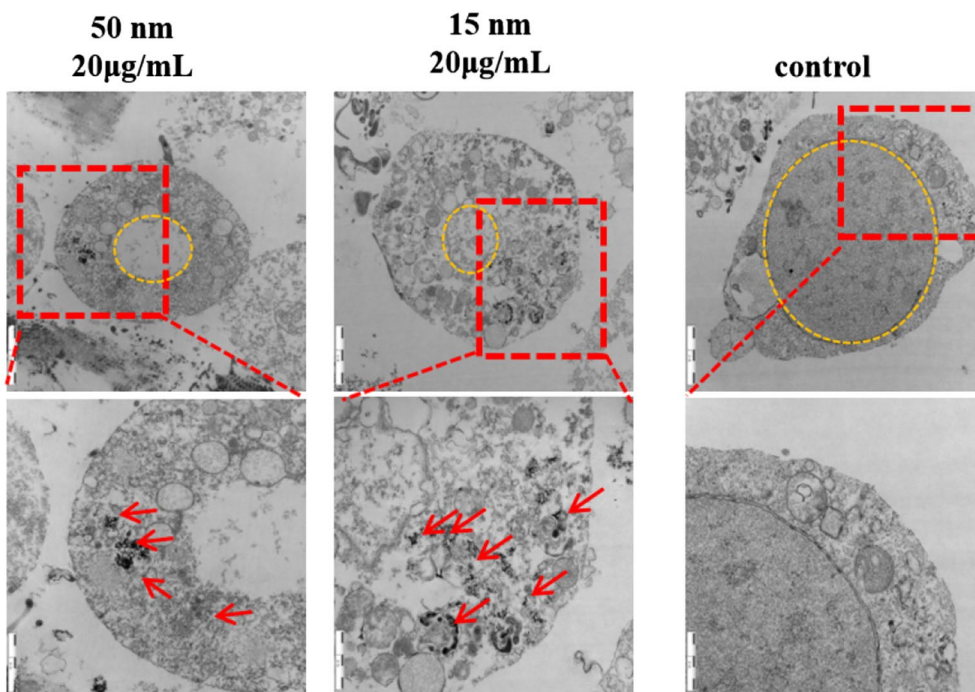


Fig. 5 TEM evaluation of the cellular uptake and localization of 15- and 50-nm SiO₂ NPs in R28 cells over 12 h. Scale bars: 1 µm and 2 µm

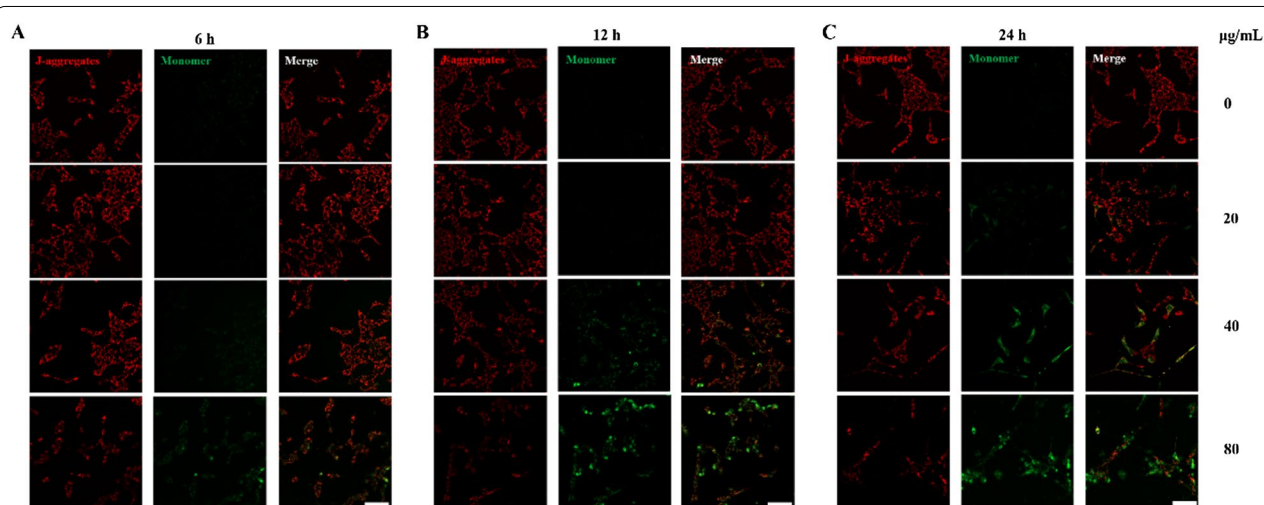
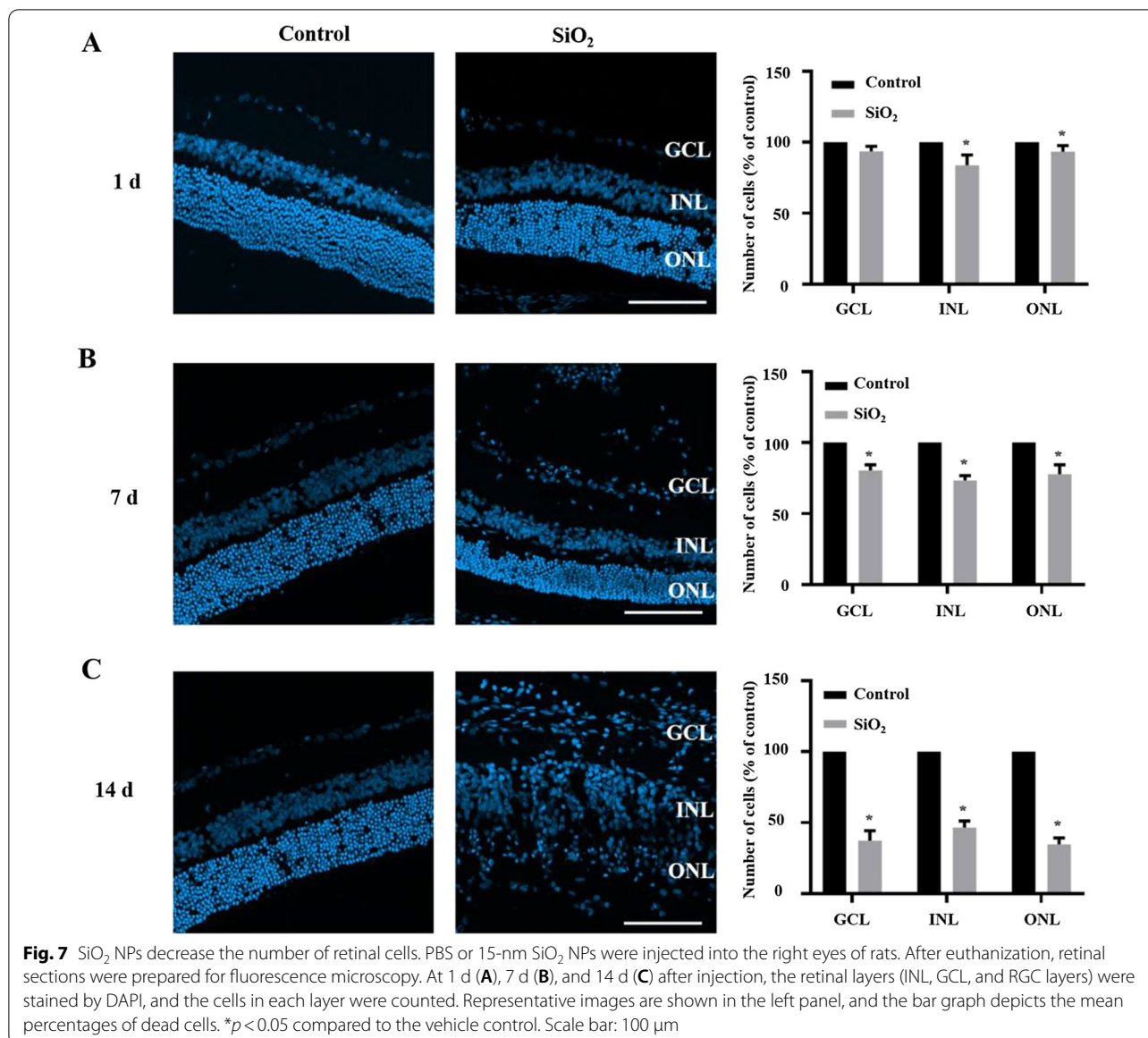


Fig. 6 SiO₂ NPs induce mitochondrial dysfunction. R28 cells were treated with three concentrations (20, 40, and 80 µg/mL) of SiO₂ NPs for 6 h (A), 12 h (B) and 24 h (C), and mitochondrial membrane potential was evaluated by JC-1 staining. Scale bar: 50 µm

Recently, SiO₂ NPs have shown great potential in the treatment of ocular diseases [36–39]. Given the widespread use of SiO₂ NPs to treat ocular diseases, the ocular toxicity of SiO₂ NPs requires more attention from scientists and ophthalmologists. Park et al. reported that SiO₂ NPs with sizes of 50, 100, and 150 nm did not induce significant cytotoxicity in cultured human corneal epithelial

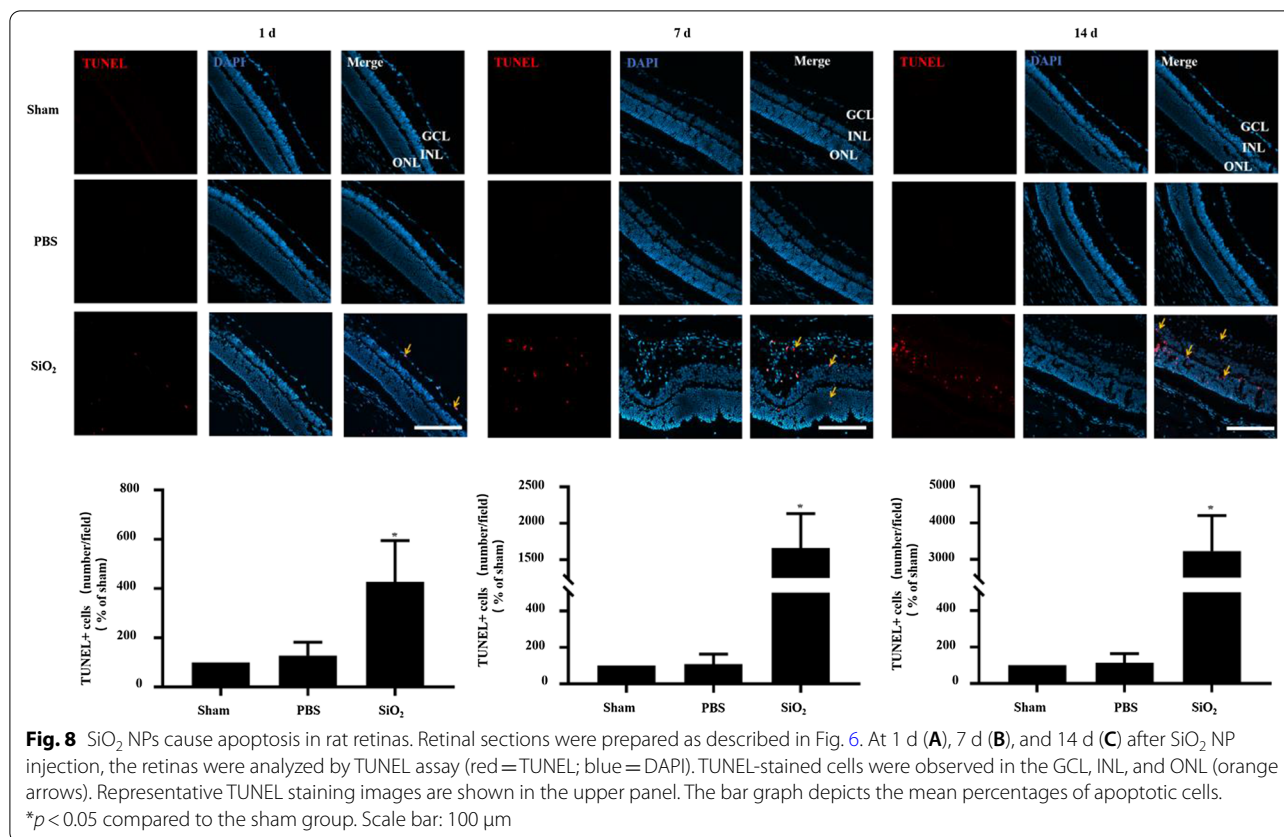
cells [40]. However, Chen et al. reported that SiO₂ NPs led to cytotoxicity, ROS generation, and DNA damage in the human cornea [15]. SiO₂ NPs can be used as intra-vitreal drug carriers [38, 41]; however, to the best of our knowledge, the retinal toxicity of SiO₂ NPs has not been investigated before now. Therefore, we conducted both in vitro and in vivo experiments to evaluate the retinal



toxicity of SiO₂ NPs with sizes of 15 and 50 nm. The *in vitro* study used human R28 retinal precursor cells, which are expected to mimic *in vivo* responses.

We first evaluated the effect of SiO₂ NP size on retinal toxicity. First, the particle morphology and average size were examined by SEM and TEM (Fig. 1). The two types of SiO₂ NPs had sizes of 15 ± 5 and 50 ± 5 nm. The images of TEM showed the slight aggregation of SiO₂ NPs. Since the toxicity of NPs depends on their phagocytosis by cells, the toxicity depends not only on their size and concentration, but also on their aggregate size and surface properties [50–52]. Hence, the hydrodynamic size distribution of NPs and zeta potential of both the NPs in distilled water, FBS-free medium, medium + 1%FBS, and medium + 10%FBS were further analyzed (Tables 1

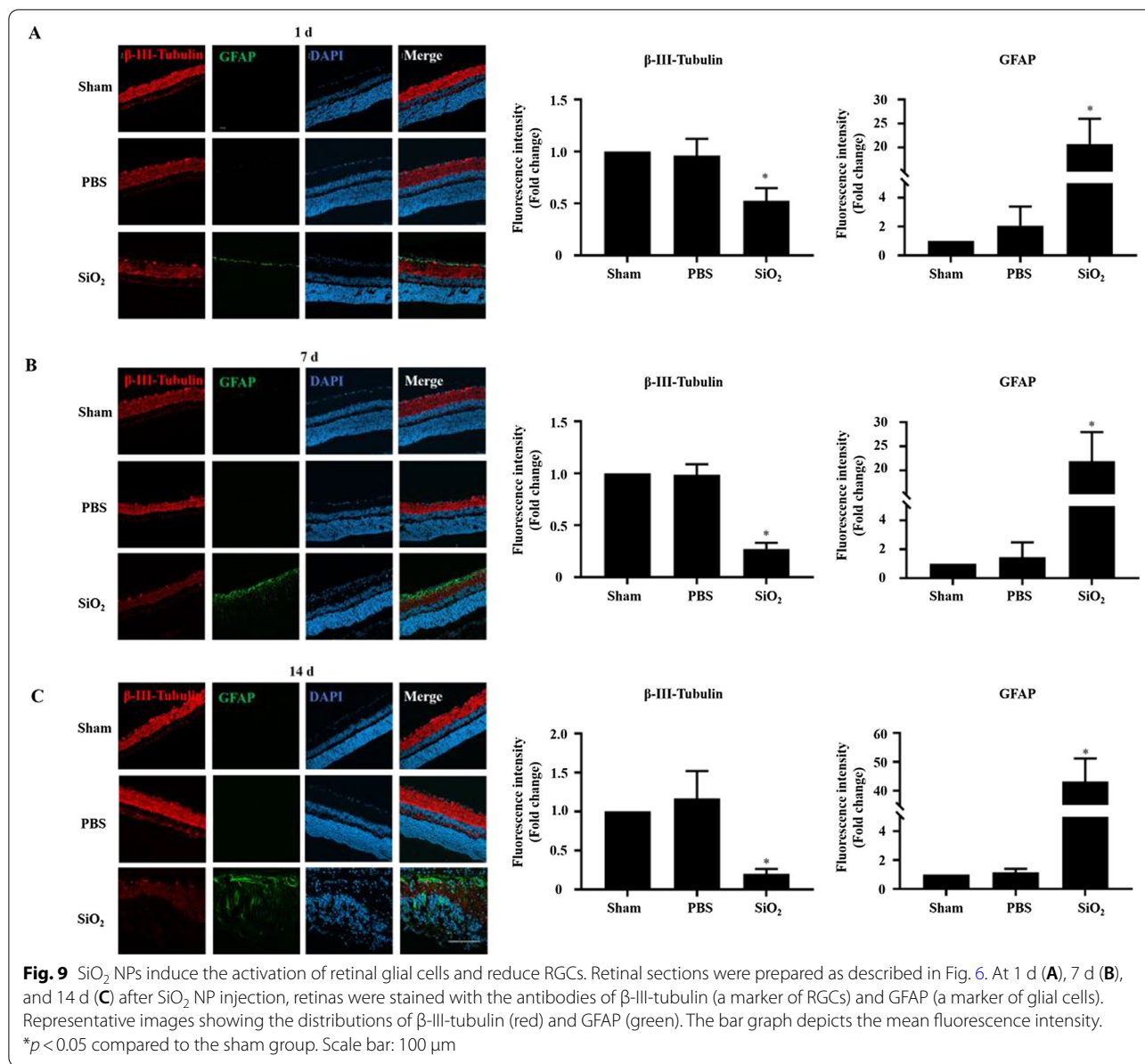
and 2). The results indicated that DMEM + FBS promoted the aggregation of NPs. This result is similar with an earlier study [53], showing that buffered solutions promote protein adsorption onto NPs and particle agglomeration. By contrast, another study reported that exposure to FBS decreased the aggregate size of titanium dioxide (TiO₂) nanoparticles, affecting the uptake and consequent effects of A549 and H1299 cells, however, this decreased of aggregation reduce the TiO₂-induced cytotoxicity. Furthermore, it has been reported that 10% FBS in cell culture medium decreased the cytotoxicity of graphene oxide (GO) in A549 cells, and this decrease is due to the adsorption of GO by FBS [52]. Interestingly, an antibacterial study of graphene showed that in the graphene sheets-melatonin-bacterial suspension,



aggregation of the sheets resulted in inactivation of *E. coli* bacteria. In our study, to avoid the affection of FBS and aggregation, the NPs in FBS-free culture medium were sonicated for 40 min in ice-bath before all treatments [54]. The 15 nm particles showed greater toxicity in R28 cells than the 50 nm particles (Figs. 3 and 4), consistent with previous studies on the effect of NP size on toxicity [1, 11, 55]. TEM imaging that both sizes of SiO₂ NPs were taken up by R28 cells within 24 h and localized within the cytoplasm (Fig. 5). Importantly, the 15-nm SiO₂ NPs were found in the mitochondria in addition to in the cytoplasm, which may explain why the 15-nm SiO₂ NPs were more toxic than the 50-nm particles. Several studies have shown that nanomaterials including SiO₂ NPs and graphene oxide nanowalls (GONWs) can damage cell membranes. For example, Bauer et al. [56] reported that SiO₂ NPs were found on the cell membrane outside the cells after exposure for 2 h, and entered the cytoplasm within 24 h of incubation, which monitored by three-dimensional atomic force microscopy and fluorescence microscopy. Shinto et al. [57] found that cell membrane disruption induced by SiO₂ NPs in different types of cells, including erythrocytes, lymphocytes, malignant melanocytes, and macrophages. In subsequent study, they found that interfacial serum proteins reduced

the membranolysis [58]. An in vitro study using bacteria demonstrated that GONWs exhibited antibacterial activity due to their sharp edges that can interact with cell membranes [59]. In contrast, it is difficult to detect the damage to the cell membrane caused by SiO₂ NPs by TEM in our study. Chen et al. [60] observed 70-nm SiO₂ NPs in the nuclei of human epithelial HEP-2 cell; however, in the our study, the nuclear translocation of SiO₂ NPs was not observed. The localization of NPs in cells can cause changes in cell morphology [61]. Thus, we evaluated the effects of the 15- and 50-nm SiO₂ NPs on R28 cell morphology. Treatment with SiO₂ NPs led to size-, time-, and concentration-dependent decreases in cell density and caused the cell shape to become ambiguous (Fig. 4).

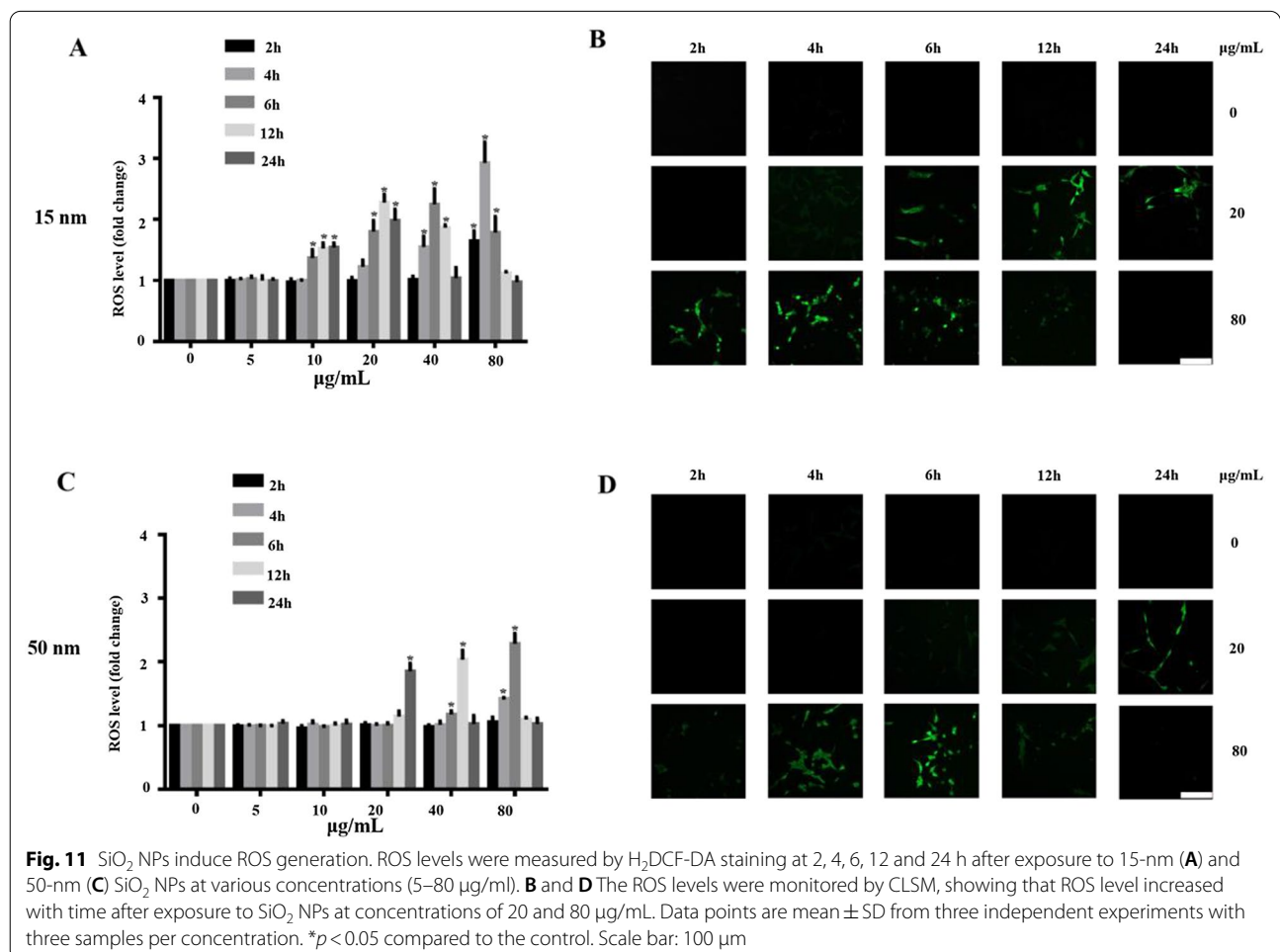
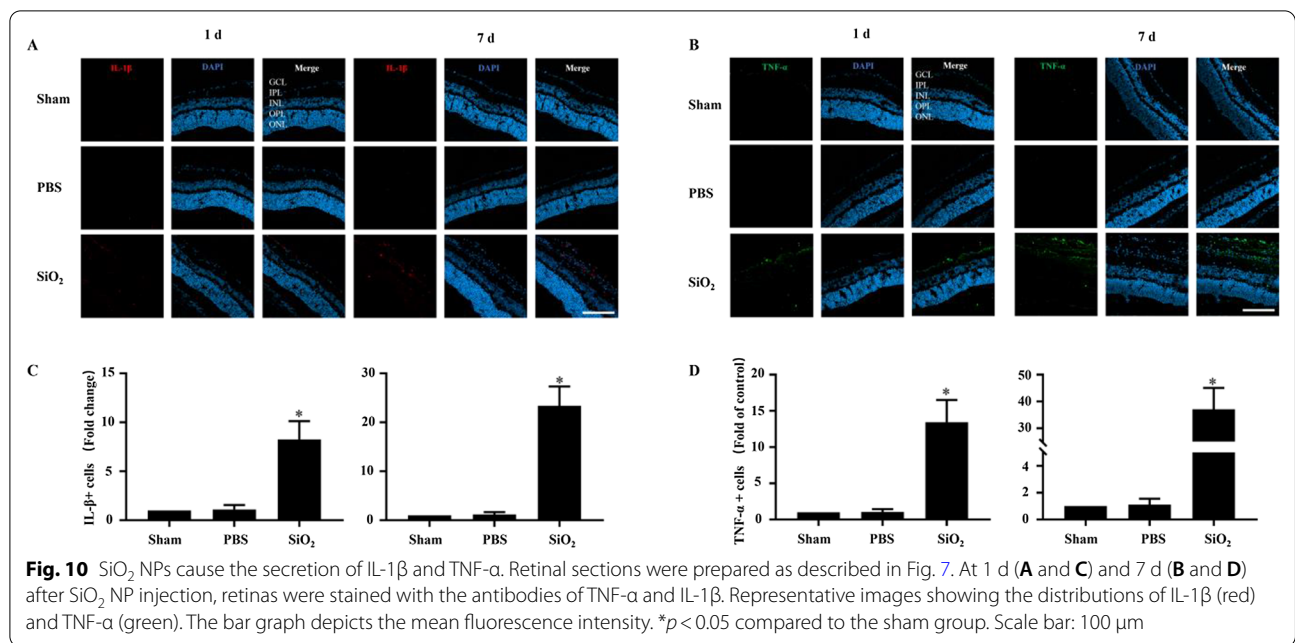
As mentioned above, the 15-nm SiO₂ NPs were more toxic than the 50-nm particles, consistent with previous studies finding that smaller particles tend to have higher cytotoxicity than larger particles. Thus, subsequent toxicity assays focused on the 15-nm SiO₂ NPs. Mitochondria play a key role in cell survival and are the primary location of ATP production. Mitochondrial depolarization can lead to a decrease in ATP level. In this study, the SiO₂ NPs induced mitochondrial dysfunction (Fig. 6). This finding is in good agreement with observations

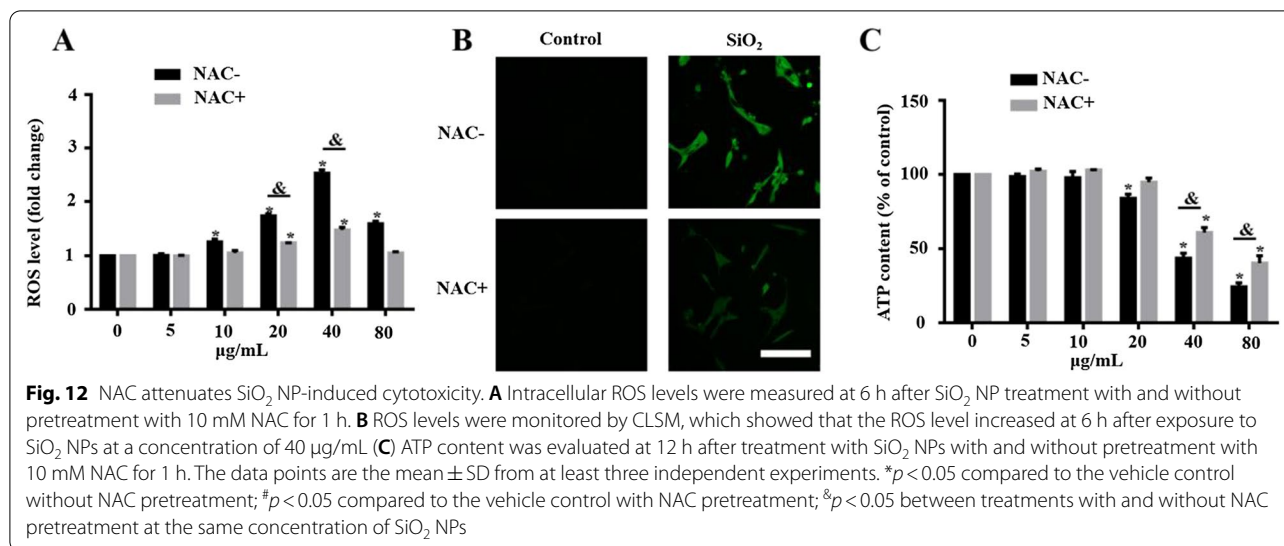


from previous studies [62, 63], where SiO₂ NP-induced cellular damage was attributed to their mitochondrial dysfunction.

Because the concentration of SiO₂ NPs used as a drug carrier was reported to be 100 μg/mL [38], we studied the in vivo retinal toxicity of SiO₂ NPs at a concentration of 80 μg/mL, which was the highest concentration used in our in vitro experiments. First, cell death and TUNEL assays were performed. Consistent with the in vitro results, the SiO₂ NPs showed time-dependent toxicity in the retina (Figs. 7 and 8). This is similar to an earlier study that reported the toxicity of SiO₂ NPs (100 nm) and TiO₂ NPs (100 nm) in R28 cells and retina [64]. As stated

by the researchers of this study, there are some limitations, which are (1) only one size of NPs was studied; (2) apoptosis was only detected in in vivo studies, but functional relevance was not assessed. Notably, our study just makes up for their limitations. We compared the toxicity of 15- and 50-nm SiO₂ NPs in two different retinal cell lines. More importantly, in our in vivo study, in addition to detecting apoptosis in various layers of the retina, we also detected damage to RGCs, which is very important for blindness. Furthermore, our results strongly indicate inflammatory cells were observed in the GCL (Figs. 7 and 8). Inflammation is the key factor in RGC damage. Our own results strengthen the idea that the injection





of SiO₂ NPs induced glial cell activation and RGC damage in a time-dependent manner (Fig. 9). In addition, our data indicate that the injection of SiO₂ NPs induced the pro-inflammatory cytokines TNF- α and IL-1 β (Fig. 10). Therefore, inflammation may be a factor in the retinal toxicity induced by SiO₂ NPs.

Oxidative stress is the most studied factor in NP-induced toxicity because the small sizes and large surface areas of NPs are thought to generate ROS and induce oxidative stress [65]. After the cell is adversely stimulated, the mitochondria produce excess ROS due to an imbalance between ROS formation and the activity of the cellular antioxidant system. If the ROS cannot be completely degraded, the excess ROS will cause oxidative stress and induce cytotoxicity, leading to cell death [66]. Recent studies found that amorphous SiO₂ led to ROS generation in MRC-5 human lung fibroblast cells [49] and MH-S macrophage cells [67]. Similar to this study, the present study demonstrated that 15- and 50-nm SiO₂ NPs caused ROS generation in R28 cells in a size- and dose-dependent manner for the first time (Fig. 11). It is worth noting that, Akhavan et al. reported that Graphene/CuO₂ nanoshuttles can release oxygen and capture respiratory electrons, and transfer them to oxygen nanobubbles, resulting in the generation of ROS and antibacterial effects. Unfortunately, SiO₂ NPs can hardly release oxygen because they have only -oh chemical bonds and no loose oxygen to release (Fig. 2). Nonetheless, XPS revealed the presence of Si(III) in the nanoparticles (Fig. 2), which is reported to be one of the reasons for the generation of ROS [42]. However, it has been reported that SiO₂ NPs can't generate ROS in cell-free

condition [68]. Our own results strengthen the endpoint that the impact of SiO₂ NPs on cells is directly correlated with their cellular uptake (Fig. 5) as the NPs induce mitochondrial dysfunction (Fig. 6), which in the main course of ROS generation. Furthermore, the SiO₂ NP-induced cytotoxicity in R28 cells was attenuated by pretreating the cells with NAC, an antioxidant (Fig. 12). This finding is in good agreement with a previous study in which cellular damage in vascular endothelial cells was attributed to the pro-oxidant effect of SiO₂ NPs [4]. Our previous study has shown that ROS can induce DNA damage, which is one of the mechanisms involved in the cytotoxicity [32]. Interestingly, the similar mechanistic insight was also found in nanomaterial-induced toxicity. For example, it was found that carbon black (CB), single wall carbon nanotube, SiO₂ and zinc dioxide (ZnO) nanoparticles can induce cytotoxicity, oxidative stress and DNA damage; however, their relationship has not been studied [69]. In subsequent studies of this line, several data and reports from in vitro studies suggest that DNA damage induced by SiO₂ NPs is mediated by oxidative stress [70–72]. Besides SiO₂, graphene nanoplatelets has also been reported to exhibit size-dependent ROS generation and genotoxicity in human stem cells [73]. It was found that cerium oxide NP-induced genotoxicity and apoptosis are mediated by ROS generation [74]. Consistent with this result, this mechanism can also be found in the toxicity induced by other metal NPs such as iron oxide [75], aluminum oxide [76], gold [77], and titanium dioxide NPs [78]. However, the research on the signaling pathways of SiO₂ and other NP-induced toxicity is still limited, and additional studies are needed in the future.

Conclusions

In summary, in the current study, both 15- and 50-nm SiO₂ NPs induced cytotoxicity in R28 cells in vitro. Based on the decrease in ATP, LDH release, localization in the mitochondria, and ROS generation, the 15-nm SiO₂ NPs were more toxic than the 50-nm NPs. The 15-nm SiO₂ NPs also induced retinal toxicity and activated inflammatory response in vivo. ROS overproduction seems to play a critical role in the retinal toxicity induced by SiO₂ NPs. The results provide new insights into the mechanism of SiO₂ NP-induced retinal toxicity and improve our understanding of the potential hazards associated with the use of SiO₂ NPs. It should be noted that this study did not consider the effects of SiO₂ NPs on signaling pathways. Additional studies are needed to better understand the contribution of signaling pathways to SiO₂ NP-induced retinal toxicity.

Supplementary Information

The online version contains supplementary material available at <https://doi.org/10.1186/s12951-022-01326-8>.

Additional file 1: Figure S1. SiO₂ NPs induce cytotoxicity in ARPE-19 cells. ARPE-19 cells were exposed to different concentrations (5–80 µg/mL) of SiO₂ NPs for (A and C) 12 h and (B and D) 24 h before measurements of (A and B) ATP content and (C and D) LDH release. Data points represent the mean ± SD from three independent experiments with three samples per concentration in each experiment. **p* < 0.05 compared to the control.

Acknowledgements

We thank Dr. Jianchao Sun for the support towards the analysis of XPS results.

Authors' contributions

ZZ: supervision and writing. LZ: investigation. YM, JL and YH: methodology. XF, SP and XW: data curation. YY, XZ and WD: methodology and data curation. JY and YZ: editing. HY: supervision and editing. SY: supervision and methodology. All authors read and approved the final manuscript.

Funding

This work was supported by funding from the National Natural Science Foundation of China (81970826 to Zhuhong Zhang and 22075241 to Shubin Yang) and the Talent Induction Program for Youth Innovation Teams in Colleges and University of Shandong Province (awarded to Yanping Zhu).

Availability of data and materials

All data generated or analyzed during this study are included in this published article.

Declarations

Ethics approval and consent to participate

All animal procedures were carried out in accordance with the National Institutes of Health Guide for the Care and Use of Laboratory Animals and were in compliance with the ARVO Statement for the Use of Animals in Ophthalmic and Vision Research. Animal protocols were approved by the Committee of Yantai University for the Care and Use of Laboratory Animals. All the procedures in this study were approved.

Consent for publication

Not applicable.

Competing interests

The authors declare no conflict of interest.

Received: 24 December 2021 Accepted: 24 February 2022

Published online: 19 March 2022

References

- Liu X, Lu B, Fu J, Zhu X, Song E, Song Y. Amorphous silica nanoparticles induce inflammation via activation of NLRP3 inflammasome and HMGB1/TLR4/MYD88/NF- κ B signaling pathway in HUVEC cells. *J Hazard Mater*. 2021;404:124050.
- Vance ME, Kuiken T, Vejerano EP, McGinnis SP, Hochella MF Jr, Rejeski D, Hull MS. Nanotechnology in the real world: redeveloping the nanomaterial consumer products inventory. *Beilstein J Nanotechnol*. 2015;6:1769–80.
- Murugadoss S, Lison D, Godderis L, Van Den Brule S, Mast J, Brassinne F, Sebaihi N, Hoet PH. Toxicology of silica nanoparticles: an update. *Arch Toxicol*. 2017;91:2967–3010.
- Sun JG, Jiang Q, Zhang XP, Shan K, Liu BH, Zhao C, Yan B. Mesoporous silica nanoparticles as a delivery system for improving antiangiogenic therapy. *Int J Nanomed*. 2019;14:1489–501.
- Yang X, Liu J, He H, Zhou L, Gong C, Wang X, Yang L, Yuan J, Huang H, He L, et al. SiO₂ nanoparticles induce cytotoxicity and protein expression alteration in HaCaT cells. *Part Fibre Toxicol*. 2010;7:1.
- Wu X, Wu M, Zhao JX. Recent development of silica nanoparticles as delivery vectors for cancer imaging and therapy. *Nanomedicine*. 2014;10:297–312.
- Hu C, Sun J, Zhang Y, Chen J, Lei Y, Sun X, Deng Y. Local delivery and sustained-release of nitric oxide donor loaded in mesoporous silica particles for efficient treatment of primary open-angle glaucoma. *Adv Healthc Mater*. 2018;7:e1801047.
- Jo DH, Kim JH, Yu YS, Lee TG, Kim JH. Antiangiogenic effect of silicate nanoparticle on retinal neovascularization induced by vascular endothelial growth factor. *Nanomedicine*. 2012;8:784–91.
- Panas A, Marquardt C, Nalcaci O, Bockhorn H, Baumann W, Paur HR, Mulhopt S, Diabate S, Weiss C. Screening of different metal oxide nanoparticles reveals selective toxicity and inflammatory potential of silica nanoparticles in lung epithelial cells and macrophages. *Nanotoxicology*. 2013;7:259–73.
- Lee SY, Kim IY, Heo MB, Moon JH, Son JG, Lee TG. Global proteomics to study silica nanoparticle-induced cytotoxicity and its mechanisms in HepG2 cells. *Biomolecules*. 2021;11:375.
- Sergent JA, Paget V, Chevillard S. Toxicity and genotoxicity of nano-SiO₂ on human epithelial intestinal HT-29 cell line. *Ann Occup Hyg*. 2012;56:622–30.
- Brandao F, Costa C, Bessa MJ, Dumortier E, Debacq-Chainiaux F, Hubaux R, Salmon M, Laloy J, Stan MS, Hermenean A, et al. Genotoxicity and gene expression in the rat lung tissue following instillation and inhalation of different variants of amorphous silica nanomaterials (aSiO₂ NM). *Nanomaterials (Basel)*. 2021;11:1502.
- Abdel-Latif HMR, Shukry M, El Euony OI, Mohamed Soliman M, Noreldin AE, Ghetas HA, Dawood MAO, Khallaf MA. Hazardous effects of SiO₂ nanoparticles on liver and kidney functions, histopathology characteristics, and transcriptomic responses in Nile Tilapia (*Oreochromis niloticus*) Juveniles. *Biology (Basel)*. 2021;10:183.
- Wang JJ, Sanderson BJ, Wang H. Cytotoxicity and genotoxicity of ultrafine crystalline SiO₂ particulate in cultured human lymphoblastoid cells. *Environ Mol Mutagen*. 2007;48:151–7.
- Chen X, Zhu S, Hu X, Sun D, Yang J, Yang C, Wu W, Li Y, Gu X, Li M, et al. Toxicity and mechanism of mesoporous silica nanoparticles in eyes. *Nanoscale*. 2020;12:13637–53.
- Bourges JL, Gautier SE, Delie F, Bejjani RA, Jeanny JC, Gurny R, BenEzra D, Behar-Cohen FF. Ocular drug delivery targeting the retina and retinal pigment epithelium using polylactide nanoparticles. *Invest Ophthalmol Vis Sci*. 2003;44:3562–9.
- Novack GD. Pharmacotherapy for the treatment of choroidal neovascularization due to age-related macular degeneration. *Annu Rev Pharmacol Toxicol*. 2008;48:61–78.

18. Penha FM, Rodrigues EB, Maia M, Furlani BA, Regatieri C, Melo GB, Magalhaes O Jr, Manzano R, Farah ME. Retinal and ocular toxicity in ocular application of drugs and chemicals—part II: retinal toxicity of current and new drugs. *Ophthalmic Res.* 2010;44:205–24.
19. Bhatnagar P, Spaide RF, Takahashi BS, Peragallo JH, Freund KB, Klancnik JM Jr, Cooney MJ, Slakter JS, Sorenson JA, Yannuzzi LA. Ranibizumab for treatment of choroidal neovascularization secondary to age-related macular degeneration. *Retina.* 2007;27:846–50.
20. Yu HJ, Ehlers JP, Sevji DD, Hach J, O'Connell M, Reese JL, Srivastava SK, Wykoff CC. Real-time photographic- and fluorescein angiographic-guided management of diabetic retinopathy: randomized PRIME trial outcomes. *Am J Ophthalmol.* 2021;226:126–36.
21. Tsang SH, Sharma T. Drug-induced retinal toxicity. *Adv Exp Med Biol.* 2018;1085:227–32.
22. Quan JH, Gao FF, Ismail H, Yuk JM, Cha GH, Chu JQ, Lee YH. Silver nanoparticle-induced apoptosis in ARPE-19 cells is inhibited by *Toxoplasma gondii* pre-infection through suppression of NOX4-dependent ROS generation. *Int J Nanomed.* 2020;15:3695–716.
23. Wang L, Chen C, Guo L, Li Q, Ding H, Bi H, Guo D. Zinc oxide nanoparticles induce murine photoreceptor cell death via mitochondria-related signaling pathway. *Artif Cells Nanomed Biotechnol.* 2018;46:1102–13.
24. Zhu S, Gong L, Li Y, Xu H, Gu Z, Zhao Y. Safety assessment of nanomaterials to eyes: an important but neglected issue. *Adv Sci (Weinh).* 2019;6:1802289.
25. Leung CC, Yu IT, Chen W. Silicosis. *Lancet.* 2012;379:2008–18.
26. Yoshida T, Yoshioka Y, Takahashi H, Misato K, Mori T, Hirai T, Nagano K, Abe Y, Mukai Y, Kamada H, et al. Intestinal absorption and biological effects of orally administered amorphous silica particles. *Nanoscale Res Lett.* 2014;9:532.
27. Tassinari R, Martinelli A, Valeri M, Maranghi F. Amorphous silica nanoparticles induced spleen and liver toxicity after acute intravenous exposure in male and female rats. *Toxicol Ind Health.* 2021; 7482337211010579.
28. Rafiepour A, Azari MR, Jaktaji PJ, Khodaghholi F, Peirovi H, Mehrabi Y, Mohammadian Y. The effect of particle size on the cytotoxicity of amorphous silicon dioxide: an in vitro toxicological study. *Asian Pac J Cancer Prev.* 2021;22:325–32.
29. Kim IY, Joachim E, Choi H, Kim K. Toxicity of silica nanoparticles depends on size, dose, and cell type. *Nanomedicine.* 2015;11:1407–16.
30. Nabeshi H, Yoshikawa T, Matsuyama K, Nakazato Y, Tochigi S, Kondoh S, Hirai T, Akase T, Nagano K, Abe Y, et al. Amorphous nanosilica induce endocytosis-dependent ROS generation and DNA damage in human keratinocytes. *Part Fibre Toxicol.* 2011;8:1.
31. Passagne I, Morille M, Rousset M, Pujalte I, LAzou B. Implication of oxidative stress in size-dependent toxicity of silica nanoparticles in kidney cells. *Toxicology.* 2012;299:112–24.
32. Zhang Z, Ren Z, Chen S, Guo X, Liu F, Guo L, Mei N. ROS generation and JNK activation contribute to 4-methoxy-TEMPO-induced cytotoxicity, autophagy, and DNA damage in HepG2 cells. *Arch Toxicol.* 2018;92:717–28.
33. Gunes S, He Z, van Acken D, Malone R, Cullen PJ, Curtin JF. Platinum nanoparticles inhibit intracellular ROS generation and protect against cold atmospheric plasma-induced cytotoxicity. *Nanomedicine.* 2021;36:102436.
34. Ma Y, Li P, Zhao L, Liu J, Yu J, Huang Y, Zhu Y, Li Z, Zhao R, Hua S, et al. Size-dependent cytotoxicity and reactive oxygen species of cerium oxide nanoparticles in human retinal pigment epithelia cells. *Int J Nanomed.* 2021;16:5333–41.
35. Abbasi F, Samaei MR, Hashemi H, Savardashtaki A, Azhdarpoor A, Fallahi MJ, Jalili M, Billet S. The toxicity of SiO₂ NPs on cell proliferation and cellular uptake of human lung fibroblastic cell line during the variation of calcination temperature and its modeling by artificial neural network. *J Environ Health Sci Eng.* 2021;19:985–95.
36. Tisi A, Passacantando M, Lozzi L, Riccitelli S, Bisti S, Maccaroni R. Retinal long term neuroprotection by Cerium Oxide nanoparticles after an acute damage induced by high intensity light exposure. *Exp Eye Res.* 2019;182:30–8.
37. Wong LL, Pye QN, Chen L, Seal S, McGinnis JF. Defining the catalytic activity of nanoceria in the P23H-1 rat, a photoreceptor degeneration model. *PLoS One.* 2015;10:e0121977.
38. Paiva MRB, Andrade GF, Dourado LFN, Castro BFM, Fialho SL, Sousa EMB, Silva-Cunha A. Surface functionalized mesoporous silica nanoparticles for intravitreal application of tacrolimus. *J Biomater Appl.* 2021;35:1019–33.
39. Qu W, Meng B, Yu Y, Wang S. Folic acid-conjugated mesoporous silica nanoparticles for enhanced therapeutic efficacy of topotecan in retina cancers. *Int J Nanomed.* 2018;13:4379–89.
40. Park JH, Jeong H, Hong J, Chang M, Kim M, Chuck RS, Lee JK, Park CY. The effect of silica nanoparticles on human corneal epithelial cells. *Sci Rep.* 2016;6:37762.
41. Wang C, Hou H, Nan K, Sailor MJ, Freeman WR, Cheng L. Intravitreal controlled release of dexamethasone from engineered microparticles of porous silicon dioxide. *Exp Eye Res.* 2014;129:74–82.
42. Yang Y, Faust JJ, Schoepf J, Hristovski K, Capco DG, Herckes P, Westerhoff P. Survey of food-grade silica dioxide nanomaterial occurrence, characterization, human gut impacts and fate across its lifecycle. *Sci Total Environ.* 2016;565:902–12.
43. Jannesari M, Akhavan O, Madaah Hosseini HR, Bakhshi B. Graphene/CuO₂ nanoshuttles with controllable release of oxygen nanobubbles promoting interruption of bacterial respiration. *ACS Appl Mater Interfaces.* 2020;12:35813–25.
44. Wang J, Wang Z, Huang B, Ma Y, Liu Y, Qin X, Zhang X, Dai Y. Oxygen vacancy induced band-gap narrowing and enhanced visible light photocatalytic activity of ZnO. *ACS Appl Mater Interfaces.* 2012;4:4024–30.
45. Bhattacharjee S. DLS and zeta potential—what they are and what they are not? *J Control Release.* 2016;235:337–51.
46. Karunakaran G, Suriyaprabha R, Rajendran V, Kannan N. Effect of contact angle, zeta potential and particles size on the in vitro studies of Al₂O₃ and SiO₂ nanoparticles. *IET Nanobiotechnol.* 2015;9:27–34.
47. Patel VR, Agrawal YK. Nanosuspension: an approach to enhance solubility of drugs. *J Adv Pharm Technol Res.* 2011;2:81–7.
48. Sung MS, Heo H, Eom GH, Kim SY, Piao H, Guo Y, Park SW. HDAC2 regulates glial cell activation in ischemic mouse retina. *Int J Mol Sci.* 2019;20:5159.
49. Petrache Voicu SN, Dinu D, Sima C, Hermenean A, Ardelean A, Codrici E, Stan MS, Zarnescu O, Dinischiotu A. Silica nanoparticles induce oxidative stress and autophagy but not apoptosis in the MRC-5 cell line. *Int J Mol Sci.* 2015;16:29398–416.
50. Il'Ves VG, Zuev MG, Sokovnin SY. Properties of silicon dioxide amorphous nanopowder produced by pulsed electron beam evaporation. *J Nanotechnol.* 2015;2015:1–8.
51. Hu J, Wang J, Liu S, Zhang Z, Zhang H, Cai X, Pan J, Liu J. Effect of TiO₂ nanoparticle aggregation on marine microalgae *Isochrysis galbana*. *J Environ Sci (China).* 2018;66:208–15.
52. Hu W, Peng C, Lv M, Li X, Zhang Y, Chen N, Fan C, Huang Q. Protein corona-mediated mitigation of cytotoxicity of graphene oxide. *ACS Nano.* 2011;5:3693–700.
53. Givens BE, Wilson E, Fiegel J. The effect of salts in aqueous media on the formation of the BSA corona on SiO₂ nanoparticles. *Colloids Surf B Biointerfaces.* 2019;179:374–81.
54. Akhavan O, Ghaderi E, Esfandiari A. Wrapping bacteria by graphene nanosheets for isolation from environment, reactivation by sonication, and inactivation by near-infrared irradiation. *J Phys Chem B.* 2011;115:6279–88.
55. Park MV, Neigh AM, Vermeulen JP, de la Fonteyne LJ, Verharen HW, Briede JJ, van Loveren H, de Jong WH. The effect of particle size on the cytotoxicity, inflammation, developmental toxicity and genotoxicity of silver nanoparticles. *Biomaterials.* 2011;32:9810–7.
56. Bauer AT, Strozzyk EA, Gorzelanny C, Westerhausen C, Desch A, Schneider MF, Schneider SW. Cytotoxicity of silica nanoparticles through exocytosis of von Willebrand factor and necrotic cell death in primary human endothelial cells. *Biomaterials.* 2011;32:8385–93.
57. Shinto H, Fukasawa T, Yoshisue K, Tezuka M, Orita MJAPT: Cell membrane disruption induced by amorphous silica nanoparticles in erythrocytes, lymphocytes, malignant melanocytes, and macrophages. *Adv Power.* 2014;25:1872.
58. Shinto H, Fukasawa T, Yoshisue K, Tsukamoto N, Aso S, Hirohashi Y, Seto H. Effect of interfacial serum proteins on the cell membrane disruption induced by amorphous silica nanoparticles in erythrocytes, lymphocytes, malignant melanocytes, and macrophages. *Colloids Surf B Biointerfaces.* 2019;181:270–7.

59. Akhavan O, Ghaderi E. Toxicity of graphene and graphene oxide nanowalls against bacteria. *ACS Nano*. 2010;4:5731–6.
60. Chen M, von Mikecz A. Formation of nucleoplasmic protein aggregates impairs nuclear function in response to SiO₂ nanoparticles. *Exp Cell Res*. 2005;305:51–62.
61. Mittal S, Pandey AK. Cerium oxide nanoparticles induced toxicity in human lung cells: role of ROS mediated DNA damage and apoptosis. *Biomed Res Int*. 2014;2014:891934.
62. Zhao X, Abulikemu A, Lv S, Qi Y, Duan J, Zhang J, Chen R, Guo C, Li Y, Sun Z. Oxidative stress- and mitochondrial dysfunction-mediated cytotoxicity by silica nanoparticle in lung epithelial cells from metabolomic perspective. *Chemosphere*. 2021;275:129969.
63. Guo C, Yang M, Jing L, Wang J, Yu Y, Li Y, Duan J, Zhou X, Li Y, Sun Z. Amorphous silica nanoparticles trigger vascular endothelial cell injury through apoptosis and autophagy via reactive oxygen species-mediated MAPK/Bcl-2 and PI3K/Akt/mTOR signaling. *Int J Nanomed*. 2016;11:5257–76.
64. Park JH, Kim DJ, Park CY. Retinal cytotoxicity of silica and titanium dioxide nanoparticles. *Toxicol Res*. 2021. <https://doi.org/10.1093/toxres/tfab117>.
65. Park EJ, Park K. Oxidative stress and pro-inflammatory responses induced by silica nanoparticles in vivo and in vitro. *Toxicol Lett*. 2009;184:18–25.
66. Moris D, Spartalis M, Tzatzaki E, Spartalis E, Karachaliou GS, Triantafyllis AS, Karaolani G, Tsilimigras DI, Theocharis S. The role of reactive oxygen species in myocardial redox signaling and regulation. *Ann Transl Med*. 2017;5:324.
67. Ghiazza M, Polimeni M, Fenoglio I, Gazzano E, Ghigo D, Fubini B. Does vitreous silica contradict the toxicity of the crystalline silica paradigm? *Chem Res Toxicol*. 2010;23:620–9.
68. Sousa CA, Soares H, Soares EV. Metal(loid) oxide (Al₂O₃, Mn₃O₄, SiO₂ and SnO₂) nanoparticles cause cytotoxicity in yeast via intracellular generation of reactive oxygen species. *Appl Microbiol Biotechnol*. 2019;103:6257–69.
69. Yang H, Liu C, Yang D, Zhang H, Xi Z. Comparative study of cytotoxicity, oxidative stress and genotoxicity induced by four typical nanomaterials: the role of particle size, shape and composition. *J Appl Toxicol*. 2009;29:69–78.
70. Tarantini A, Lancelleur R, Mourot A, Lavault M-T, Casterou G, Jarry G, Hogeveen K, Fessard V. Toxicity, genotoxicity and proinflammatory effects of amorphous nanosilica in the human intestinal Caco-2 cell line. *Toxicol In Vitro*. 2015;29:398–407.
71. Chen X, Zhu S, Hu X, Sun D, Yang J, Yang C, Wu W, Li Y, Gu X, Li MJN. Toxicity and mechanism of mesoporous silica nanoparticles in eyes. *Nanoscale*. 2020;12:13637–53.
72. Zhou F, Liao F, Chen L, Liu Y, Wang W, Feng S. The size-dependent genotoxicity and oxidative stress of silica nanoparticles on endothelial cells. *Environ Sci Pollut Res Int*. 2019;26:1911–20.
73. Akhavan O, Ghaderi E, Akhavan A. Size-dependent genotoxicity of graphene nanoplatelets in human stem cells. *Biomaterials*. 2012;33:8017–25.
74. Mittal S, Pandey AK. Cerium oxide nanoparticles induced toxicity in human lung cells: role of ROS mediated DNA damage and apoptosis. *BioMed Res Int*. 2014;204:1.
75. Fernandez-Bertozel N, Costa C, Bessa MJ, Park M, Carriere M, Dussert F, Teixeira JP, Pasaro E, Laffon B, Valdiglesias V. Assessment of oxidative damage induced by iron oxide nanoparticles on different nervous system cells. *Mutat Res Genet Toxicol Environ Mutagen*. 2019;845:402989.
76. Rajiv S, Jerobin J, Saranya V, Nainawat M, Sharma A, Makwana P, Gayathri C, Bharath L, Singh M, Kumar MJH. Toxicology e: Comparative cytotoxicity and genotoxicity of cobalt (II, III) oxide, iron (III) oxide, silicon dioxide, and aluminum oxide nanoparticles on human lymphocytes in vitro. *Hum Exp Toxicol*. 2016;35:170–83.
77. May S, Hirsch C, Rippl A, Bohmer N, Kaiser J-P, Diener L, Wichser A, Bürkle A, Wick PJN. Transient DNA damage following exposure to gold nanoparticles. *Nanoscale*. 2018;10:15723–35.
78. Han B, Pei Z, Shi L, Wang Q, Li C, Zhang B, Su X, Zhang N, Zhou L, Zhao B. TiO₂ nanoparticles caused DNA damage in lung and extra-pulmonary organs through ROS-activated FOXO3a signaling pathway after intratracheal administration in rats. *Int J Nanomed*. 2020;15:6279.

Publisher's Note

Springer Nature remains neutral with regard to jurisdictional claims in published maps and institutional affiliations.

Ready to submit your research? Choose BMC and benefit from:

- fast, convenient online submission
- thorough peer review by experienced researchers in your field
- rapid publication on acceptance
- support for research data, including large and complex data types
- gold Open Access which fosters wider collaboration and increased citations
- maximum visibility for your research: over 100M website views per year

At BMC, research is always in progress.

Learn more biomedcentral.com/submissions

